Multibody Syst Dyn (2017) 40:123–153
DOI 10.1007/s11044-016-9532-9

Energy-efficacy comparisons and multibody dynamics analyses of legged robots with different closed-loop mechanisms

Kazuma Komoda[1] · **Hiroaki Wagatsuma**[1,2,3]

Received: 9 July 2015 / Accepted: 22 July 2016 / Published online: 20 December 2016

Abstract As for biological mechanisms, which provide a specific functional behavior, the kinematic synthesis is not so simply applicable without deep considerations on requirements, such as the ideal trajectory, fine force control along the trajectory, and possible minimization of the energy consumption. An important approach is the comparison of acknowledged mechanisms to mimic the function of interest in a simplified manner. It helps to consider why the motion trajectory is generated as an optimum, arising from a hidden biological principle on adaptive capability for environmental changes. This study investigated with systematic methods of forward and inverse kinematics known as multibody dynamics (MBD) before going to the kinematic synthesis to explore what the ideal end-effector coordinates are. In terms of walking mechanisms, there are well-known mechanisms, yet the efficacy is still unclear. The Chebyshev linkage with four links is the famous closed-loop system to mimic a simple locomotion, from the 19th century, and recently the Theo Jansen mechanism bearing 11 linkages was highlighted since it exhibited a smooth and less-energy locomotive behavior during walking demonstrations in the sand field driven by wind power. Coincidentally, Klann (1994) emphasized his closed-loop linkage with seven links to mimic a spider locomotion. We applied MBD to three walking linkages in order to compare factors arising from individual mechanisms. The MBD-based numerical computation demonstrated that the Chebyshev, Klann, and Theo Jansen mechanisms have a common property in acceleration control during separate swing and stance phases to exhibit the walking behavior, while they have different tendencies in the total energy consumption and energy-efficacy measured by the 'specific resistance'. As a consequence, this study for the first time revealed that specific resistances of three linkages exhibit a proportional relationship to the

✉ K. Komoda
komoda-kazuma@edu.brain.kyutech.ac.jp

H. Wagatsuma
waga@brain.kyutech.ac.jp

1 Graduate School of Life Science and Systems Engineering, Kyushu Institute of Technology, 2-4 Hibikino, Wakamatsu-Ku, Kitakyushu 808-0196, Japan

2 RIKEN Brain Science Institute, 2-1 Hirosawa, Wako-shi, Saitama, Japan

3 Artificial Intelligence Research Center, AIST, 2-3-26 Aomi, Koto-ku, Tokyo, Japan

walking speed, which is consistent with human walking and running, yet interestingly it is not consistent with older walking machines, like ARL monopod I, II. The results imply a similarity between biological evolution and robot design, in that the Chebyshev mechanism provides the simplest walking motion with fewer linkages and the Theo Jansen mechanism realizes a fine profile of force changes along the trajectory to reduce the energy consumption acceptable for a large body size by increasing the number of links.

Keywords Walking mechanism · Multilegged robot · Closed-loop linkage · Energy consumption · Biological motion · Specific resistance

1 Introduction

Multibody dynamics (MBD) has been developed to analyze multibody systems, finite element systems, and continuous systems in a unified manner by Schiehlen [54] based on the Kane's Method [34] and computer-aided analysis initially introduced by Nikravesh [42]. For planar and spatial systems, Haug [26] and Schiehlen [56] organized the MBD according to the generalized coordinate system for biological complex systems [59]. In a recent trend, data-driven analyses have shown a large potential [3, 19] in specifying possible coordinates from high degrees of freedom in recording data derived from the observation of biological movements, such as using principal component analysis (PCA) to reduce the number of degrees of freedom of a mechanism after the noise removal. On the other hand, the traditional model-based approach is still the fastest pathway to reach the actual physical system to build the target mechanism. Closed-linkages were frequently used to provide a specific repetitive motion by reducing the degrees of freedom, as to be bio-inspired robots, especially for walking mechanisms. The most famous mechanism is the Chebyshev linkage walking mechanism, which was developed by Pafnuty Chebyshev [10] in the 19th century. Recently Theo Jansen [31], a Dutch kinematic artist, proposed a system with 11 linkages inspired by biological evolution. The linkage effectively provided a smooth trajectory of leg motion and demonstrated a real locomotive behavior on irregular ground only using wind power. From an engineering perspective, the Klann mechanism proposed by Joe Klann [35] succeeded in reproducing a spider's locomotion. The Theo Jansen mechanism can be considered as a tool for elucidation of how the mechanism moves like an animal, which has the potential to generate a smooth trajectory and improve energy efficiency. The linkage may represent a biological mechanism with inevitable physical constraints, similar to the coupling of pulling and pushing forces; however, only limited theoretical analyses have been reported, such as the center-of-mass approximation [29] and a focused mechanical analysis [40], which did not perform any serious comparative studies with other similar walking systems. Here we introduce the MBD approach for comparing the effectiveness of movement mechanisms, including earlier proposed walking machines, using the common criterion such as the specific resistance. We hypothesized that closed-loop mechanisms have a consistent property with the energy consumption of animals and the Theo Jansen mechanism in particular maximizes the resemblance to the trajectory smoothness.

This paper is divided into the following sections. Section 2 introduces common MBD formulations. Section 3 contains model descriptions of three closed-loop mechanisms, while Sect. 4 describes their characteristic analyses including placement, posture, velocity, acceleration, and torque. Section 5 focuses on walking trajectory investigations on the duty factor, which are extended to analyses of energy consumption in Sect. 6. The final result of the comparison of specific resistances among the three closed linkages is in Sect. 7, which broadens

to the comparison with walking machines proposed in the past, including monopods, biped, quadruped, six-legged, and human walking and running behaviors. Section 8 discusses the potential and limitation. This systematic analysis is devoted to clarifying which property of the closed linkages has an advantage with respect to older walking machines, and the accomplishment of the qualitative comparison with the MBD reveals a similar property and dissimilarity of the three types, which is a clue to how biological walking mechanisms evolved.

2 Formulations of the equations of motion for legged robots with closed-loop mechanisms

In order to analyze the forward kinematics and inverse kinematics of a constrained dynamics system, it is necessary to describe the behavior of a multibody system (MBS) by using the equation of motion. The MBS is constructed by a group of rigid and flexible bodies, which depend on kinematic constraints and forces. Kinematic constraints demonstrate linear or quadratic dependence on the generalized Cartesian coordinate. Various approaches for the generation of the equation of motion in the MBS have been suggested [26, 42, 53, 58].

If a planar mechanism is made up of nb rigid bodies, the number of planar Cartesian generalized coordinates is $nc = 3 \times nb$. The vector of generalized coordinates for the systems is written as

$$\mathbf{q} = \left[\mathbf{q}_1^T, \mathbf{q}_2^T, \ldots, \mathbf{q}_{nb}^T\right]^T, \tag{1}$$

where $\mathbf{q}_i = [x_i, y_i, \theta_i]_i^T$ is the vector of planar Cartesian generalized coordinates for an MBS.

A kinematic constraint between body i and body j imposes conditions on the relative motion between the pair of bodies at an arbitrary joint k, and it is described, if it is a rotary joint, as

$$\begin{aligned}\boldsymbol{\Phi}_k^{K(i,j)} &= \left(\mathbf{r}_i + \mathbf{A}_i \mathbf{s}_i'^k\right) - \left(\mathbf{r}_j + \mathbf{A}_j \mathbf{s}_j'^k\right) \\ &= \begin{pmatrix} x_i + x_i'^k \cos\theta_i - y_i'^k \sin\theta_i - x_j - x_j'^k \cos\theta_j + y_j'^k \sin\theta_j \\ y_i + x_i'^k \sin\theta_i + y_i'^k \cos\theta_i - y_j - x_j'^k \sin\theta_j - y_j'^k \cos\theta_j \end{pmatrix} = \mathbf{0},\end{aligned} \tag{2}$$

where $\mathbf{r}_i$ is the vector to the centroid of the body, $\mathbf{A}_i$ is the rotation transformation matrix, and $\mathbf{s}_i'^k$ is the local representation of the body fixed vector to point k.

According to the configuration of the MBS defined by n vectors of generalized coordinates of $\mathbf{q}$ where t is the time, a set of kinematic constraint equations $\boldsymbol{\Phi}$ is obtained as

$$\boldsymbol{\Phi}(\mathbf{q}, t) = \begin{bmatrix} \boldsymbol{\Phi}^K(\mathbf{q}) \\ \boldsymbol{\Phi}^D(\mathbf{q}, t) \end{bmatrix} = \mathbf{0}, \tag{3}$$

where $\boldsymbol{\Phi}^K(\mathbf{q})$ is the kinematic constraint equation and $\boldsymbol{\Phi}^D(\mathbf{q}, t)$ denotes the driving constraints of the MBS.

The first derivative of Eq. (3) with respect to time is used to obtain the velocity constraint equation while the second derivative of Eq. (3) with respect to time yields the acceleration constraint equation as:

$$\boldsymbol{\Phi}_\mathbf{q} \dot{\mathbf{q}} = \boldsymbol{\upsilon}, \tag{4}$$

$$\mathbf{\Phi_q}\ddot{\mathbf{q}} = \boldsymbol{\gamma}, \tag{5}$$

where $\mathbf{\Phi_q}$ is the Jacobian matrix of the kinematic constraint equations, $\boldsymbol{\upsilon}$ is the velocity equation, and $\boldsymbol{\gamma}$ is the acceleration equation.

The equations of motion for a constrained MBS are described through the virtual power principle as shown by Nikravesh [42] and Haug [26]:

$$\mathbf{M}\ddot{\mathbf{q}} + \mathbf{\Phi}_\mathbf{q}^T\boldsymbol{\lambda} = \mathbf{g}, \tag{6}$$

where $\mathbf{M}$ is the mass matrix, $\ddot{\mathbf{q}}$ is the generalized acceleration vector, $\boldsymbol{\lambda}$ is the vector of Lagrange multipliers, and $\mathbf{g}$ is the generalized external force vector.

As for dynamics analysis, the kinematic constraint equations determine the algebraic configuration, and then dynamical behavior can be defined by the second order differential equations. Therefore, Eqs. (5) and (6) are described in the matrix form of differential-algebraic equations (DAEs) as

$$\begin{bmatrix} \mathbf{M} & \mathbf{\Phi}_q^T \\ \mathbf{\Phi}_q & \mathbf{0} \end{bmatrix} \begin{bmatrix} \ddot{\mathbf{q}} \\ \boldsymbol{\lambda} \end{bmatrix} = \begin{bmatrix} \mathbf{g} \\ \hat{\boldsymbol{\gamma}} \end{bmatrix}, \tag{7}$$

where $\hat{\boldsymbol{\gamma}} = \boldsymbol{\gamma} - 2\alpha\dot{\mathbf{\Phi}} - \beta^2\mathbf{\Phi}$ is the stabilization equation obtained by the Baumgarte stabilization method [8] with parameters $\alpha = 10$ and $\beta = \sqrt{2\alpha}$ for maintaining stability in the system [22, 62], which is truly important in effectively reducing the accumulation error in numerical simulations to obtain an accurate solution.

Since the system has only one degree of freedom, the inverse dynamic analysis introduces rearranged DAEs as

$$\tau = \frac{\dot{\mathbf{q}}'(\mathbf{M}\ddot{\mathbf{q}} - \mathbf{g})}{{}^{(d)}\mathbf{D}\dot{\mathbf{q}}} \tag{8}$$

where τ is a driving torque and ${}^{(d)}\mathbf{D}$ is the Jacobian of the driver constraints. It should be noted here that the array $\dot{q}$ does not have to contain the actual velocity components of the system [42, 43].

3 Modeling legged robots with three different closed-loop mechanisms

The common framework of preliminaries and definitions in Sect. 2 is applied to specific cases. In this section, three different closed-loop mechanisms are treated by using MBD: the Chebyshev linkage, the Klann mechanism, and the Theo Jansen mechanism. Individual DAEs allow for analysis of the placement, velocity, acceleration, and torque of these three legged robots.

3.1 Chebyshev linkage

The mathematical model for the Chebyshev linkage is illustrated in Fig. 1. The vector $\mathbf{q}$ with 18 elements including placements and attitude angles is shown as generalized coordinates as follows:

$$\mathbf{q} = \left[\mathbf{q}_1^T, \mathbf{q}_2^T, \mathbf{q}_3^T, \mathbf{q}_4^T, \mathbf{q}_5^T, \mathbf{q}_6^T\right]^T. \tag{9}$$

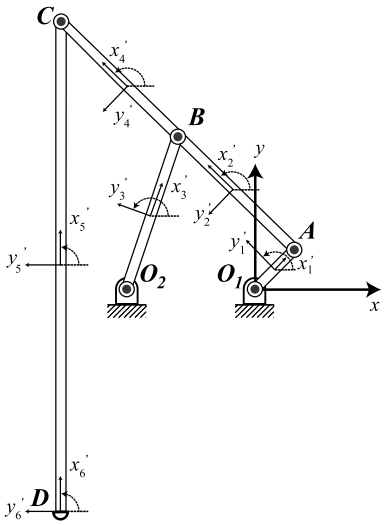

Fig. 1 Generalized coordinates on the Chebyshev linkage. This figure shows x and y coordinate axes for the rotational angle of each joint

Although the original Chebyshev linkage is known as the four link mechanism, in this comparative analysis, an attachment on the toe (the end effector) with the ground and an extension link to project the original trajectory drawing in the air onto the bottom are introduced for the purpose of comparison with other two mechanisms in a simple manner. Therefore, 18 ($= 6 \times 3$) elements are obtained in the generalized coordinates in the present analysis.

A set of kinematic constraint equations $\mathbf{\Phi}$ is given by Eq. (3). The first 17 elements of the column matrix $\mathbf{\Phi}^K(\mathbf{q})$ are derived from kinematic constraint equations. The last element $\mathbf{\Phi}^D(\mathbf{q}, t)$ is derived by the driving constraint equation, the equation of kinematic constraints and the driving constraint as shown below:

$$\mathbf{\Phi}(\mathbf{q}, t) = \begin{bmatrix} x_1 - l_1\cos\theta_1 \\ y_1 - l_1\sin\theta_1 \\ x_2 - l_2\cos\theta_2 - x_1 - l_1\cos\theta_1 \\ y_2 - l_2\sin\theta_2 - y_1 - l_1\sin\theta_1 \\ x_3 + l_3\cos\theta_3 - x_2 - l_2\cos\theta_2 \\ y_3 + l_3\sin\theta_3 - y_2 - l_2\sin\theta_2 \\ x_3 - l_3\cos\theta_3 + a \\ y_3 - l_3\sin\theta_3 \\ x_4 - l_4\cos\theta_4 - x_2 - l_2\cos\theta_2 \\ y_4 - l_4\sin\theta_4 - y_2 - l_2\sin\theta_2 \\ x_5 + l_5\cos\theta_5 - x_4 - l_4\cos\theta_4 \\ y_5 + l_5\sin\theta_5 - y_4 - l_4\sin\theta_4 \\ \theta_4 - \theta_2 \\ \theta_5 - \frac{\pi}{2} \\ x_6 - l_6\cos\theta_6 - x_5 + l_5\cos\theta_5 \\ y_6 - l_6\sin\theta_6 - y_5 + l_5\sin\theta_5 \\ \theta_6 - \theta_5 \\ \theta_1 + \omega t \end{bmatrix}_{18\times 1} = \mathbf{0}, \tag{10}$$

Table 1 Parameters of link length in the Chebyshev linkage

Parameter	Sides	Length ($\times 10^{-3}$ m)	Mass ($\times 10^{-3}$ kg)
l_1	O_1A	46.9	48.58
l_2	AB	132.2	136.84
l_3	O_2B	132.2	136.84
l_4	BC	132.2	136.84
l_5	CD	396.7	410.51
l_6	D	1.0	0.97
a	O_1O_2	207.6	–

where l_1 to l_6 are link lengths, t is time, and ω is the angular velocity of the driving link (practically called 'crankshaft') in the mechanism. Table 1 presents a set of parameter values of the Chebyshev linkage with the half-circle attachment. Parameters are normalized to be the same total weight, the same movement length at the stance phase (stride length), and the same driving link size with other two mechanisms.

The Jacobian matrix $\mathbf{\Phi}_q$ is obtained as

$$\mathbf{\Phi}_q = \left[\frac{\partial \mathbf{\Phi}(\mathbf{q}, t)}{\partial \mathbf{q}} \right]_{18\times 18}, \tag{11}$$

which allows us to investigate placement, velocity, and acceleration analyses kinematically.

In forward dynamics analysis, the mass matrix $\mathbf{M}$ (18×18) and the generalized external force vector $\mathbf{Q}^A$ (18×1) are described as follows:

$$\mathbf{M} = \mathrm{diag}(\mathbf{M}_1, \mathbf{M}_2, \ldots, \mathbf{M}_6), \tag{12}$$

$$\left\{ \mathbf{M}_i = [m_i, m_i, J_i]^T \;\middle|\; i = 1, \ldots, 6 \right\}, \tag{13}$$

$$\mathbf{Q}^A = \left[\mathbf{Q}_1^{A^T}, \mathbf{Q}_2^{A^T}, \ldots, \mathbf{Q}_6^{A^T} \right]^T, \tag{14}$$

$$\left\{ \mathbf{Q}_i^A = [0, -m_i g, 0]^T \;\middle|\; i = 1, \ldots, 6 \right\}, \tag{15}$$

where m_i is the mass of the rigid linkage to point i, $J_i = m_i l_i^2/3$ $(i = 1, \ldots, 5)$ is the polar moment of inertia of the rigid linkage to point i, g is the gravitational acceleration, and $J_6 = m_6 l_6^2/2$ is the polar moment of inertia of the half-circle attachment. In addition, the reaction force from the ground at the stance phase is given as the external force (the total mass of the mechanism) into the generalized coordinate $[x_6, y_6]$ in a numerical manner.

3.2 Klann mechanism

The mathematical model of the Klann mechanism is illustrated in Fig. 2. According to the vectors $\mathbf{q}$ with 39 elements including placements and attitude angles, the generalized coordinates are defined as follows:

$$\mathbf{q} = \left[\mathbf{q}_1^T, \mathbf{q}_2^T, \mathbf{q}_3^T, \mathbf{q}_4^T, \mathbf{q}_5^T, \mathbf{q}_6^T, \mathbf{q}_7^T, \mathbf{q}_8^T, \mathbf{q}_9^T, \mathbf{q}_{10}^T, \mathbf{q}_{11}^T, \mathbf{q}_{12}^T, \mathbf{q}_{13}^T \right]^T. \tag{16}$$

Although the original Klann mechanism is known as the system with 12 links, in this comparative analysis, an attachment with the ground and an extension link of the end-

effector for normalization of the stride length and the total size against the driving link size are introduced for the purpose of comparison with other two mechanisms in a simple manner. Therefore, 39 ($= 13 \times 3$) elements are obtained in the generalized coordinates in the present analysis.

A set of kinematic constraint equations $\mathbf{\Phi}$ is given by Eq. (3). The first 38 elements of the column matrix $\mathbf{\Phi}^K(\mathbf{q})$ are derived from kinematic constraint equations. The last element $\mathbf{\Phi}^D(\mathbf{q}, t)$ is derived by the driving constraint equation, the equation of kinematic constraints, and the driving constraint as shown below:

$$\mathbf{\Phi}(\mathbf{q}, t) = \begin{bmatrix} x_1 - l_1\cos\theta_1 \\ y_1 - l_1\sin\theta_1 \\ x_2 + l_2\cos\theta_2 - x_1 - l_1\cos\theta_1 \\ y_2 + l_2\sin\theta_2 - y_1 - l_1\sin\theta_1 \\ x_3 - l_3\cos\theta_3 - x_2 + l_2\cos\theta_2 \\ y_3 - l_3\sin\theta_3 - y_2 + l_2\sin\theta_2 \\ x_4 - l_4\cos\theta_4 - x_3 - l_3\cos\theta_3 \\ y_4 - l_4\sin\theta_4 - y_3 - l_3\sin\theta_3 \\ x_7 + l_7\cos\theta_7 - x_6 - l_6\cos\theta_6 \\ y_7 + l_7\sin\theta_7 - y_6 - l_6\sin\theta_6 \\ x_9 - l_9\cos\theta_9 - x_8 + l_8\cos\theta_8 \\ y_9 - l_9\sin\theta_9 - y_8 + l_8\sin\theta_8 \\ x_{11} - l_{11}\cos\theta_{11} - x_{10} + l_{10}\cos\theta_{10} \\ y_{11} - l_{11}\sin\theta_{11} - y_{10} + l_{10}\sin\theta_{10} \\ x_{12} + l_{12}\cos\theta_{12} - x_{11} - l_{11}\cos\theta_{11} \\ y_{12} + l_{12}\sin\theta_{12} - y_{11} - l_{11}\sin\theta_{11} \\ x_4 + l_4\cos\theta_4 - x_2 - l_2\cos\theta_2 \\ y_4 + l_4\sin\theta_4 - y_2 - l_2\sin\theta_2 \\ x_5 + l_5\cos\theta_5 - x_2 + l_2\cos\theta_2 \\ y_5 + l_5\sin\theta_5 - y_2 + l_2\sin\theta_2 \\ x_7 - l_7\cos\theta_7 - x_4 + l_4\cos\theta_4 \\ y_7 - l_7\sin\theta_7 - y_4 + l_4\sin\theta_4 \\ x_8 + l_8\cos\theta_8 - x_3 - l_3\cos\theta_3 \\ y_8 + l_8\sin\theta_8 - y_3 - l_3\sin\theta_3 \\ x_9 + l_9\cos\theta_9 - x_7 - l_7\cos\theta_7 \\ y_9 + l_9\sin\theta_9 - y_7 - l_7\sin\theta_7 \\ x_{10} + l_{10}\cos\theta_{10} \\ y_{10} + l_{10}\sin\theta_{10} \\ x_{12} + l_{12}\cos\theta_{12} \\ y_{12} + l_{12}\sin\theta_{12} \\ x_5 - l_5\cos\theta_5 - x_{10} + l_{10}\cos\theta_{10} \\ y_5 - l_5\sin\theta_5 - y_{10} + l_{10}\sin\theta_{10} \\ x_6 - l_6\cos\theta_6 - x_{12} - l_{12}\cos\theta_{12} \\ y_6 - l_6\sin\theta_6 - y_{12} - l_{12}\sin\theta_{12} \\ \theta_{11} - \frac{\pi}{2} \\ x_{13} - l_{13}\cos\theta_{13} - x_9 + l_9\cos\theta_9 \\ y_{13} - l_{13}\sin\theta_{13} - y_9 + l_9\sin\theta_9 \\ \theta_{13} - \theta_9 \\ \theta_1 + \omega t \end{bmatrix}_{39\times 1} = \mathbf{0}, \tag{17}$$

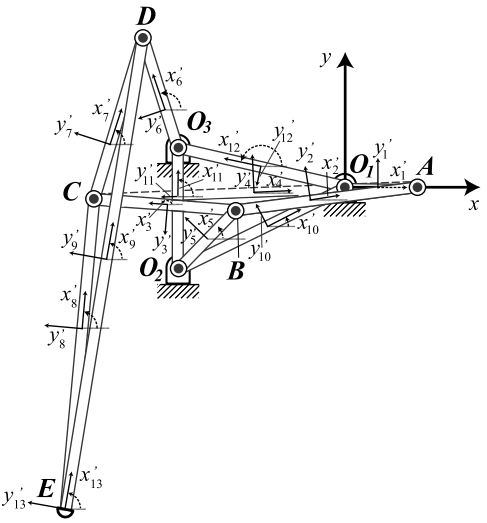

Fig. 2 Generalized coordinates on the Klann mechanism. This figure shows x and y coordinate axes for the rotational angle of each joint

Table 2 Parameters of link length and mass in the Klann mechanism

Parameter	Sides	Length ($\times 10^{-3}$ m)	Mass ($\times 10^{-3}$ kg)
l_1	O_1A	50.9	25.83
l_2	AB	133.3	67.64
l_3	BC	102.8	52.14
l_4	AC	234.8	119.13
l_5	O_2B	60.2	30.53
l_6	O_3D	84.3	42.74
l_7	CD	122.7	62.24
l_8	CE	226.8	115.08
l_9	DE	347.9	176.51
l_{10}	O_1O_2	137.1	69.57
l_{11}	O_2O_3	88.6	44.96
l_{12}	O_1O_3	126.5	64.15
l_{13}	E	1.0	0.52

where l_1 to l_{13} are link lengths, t is time, and ω is the angular velocity of the crankshaft in the mechanism. Table 2 shows a set of parameter values of the Klann mechanism with the half-circle attachment. Parameters are normalized as in the previous section.

Therefore, the Jacobian matrix $\mathbf{\Phi}_q$ is obtained as

$$\mathbf{\Phi}_q = \left[\frac{\partial \mathbf{\Phi}(\mathbf{q}, t)}{\partial \mathbf{q}} \right]_{39\times 39}, \tag{18}$$

which allows us to investigate placement, velocity, and acceleration analyses kinematically.

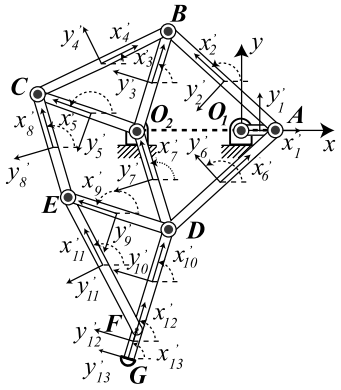

Fig. 3 Generalized coordinates on the Theo Jansen mechanism. This figure shows x and y coordinate axes for the rotational angle of each joint [36]

The forward dynamics analysis introduces the mass matrix $\mathbf{M}$ (39×39), and the generalized external force vector $\mathbf{Q}^A$ (39×1) are described as follows:

$$\mathbf{M} = \mathrm{diag}(\mathbf{M}_1, \mathbf{M}_2, \ldots, \mathbf{M}_{13}), \tag{19}$$

$$\left\{\mathbf{M}_i = [m_i, m_i, J_i]^T \;\middle|\; i = 1, \ldots, 13\right\}, \tag{20}$$

$$\mathbf{Q}^A = \left[\mathbf{Q}_1^{A^T}, \mathbf{Q}_2^{A^T}, \ldots, \mathbf{Q}_{13}^{A^T}\right]^T, \tag{21}$$

$$\left\{\mathbf{Q}_i^A = [0, -m_i g, 0]^T \;\middle|\; i = 1, \ldots, 13\right\}, \tag{22}$$

where m_i is the mass of the rigid linkage to point i, $J_i = 2l_i/3$ $(i = 1, \ldots, 12)$ is the polar moment of inertia of the rigid linkage to point i, and g is the gravitational acceleration, and $J_{13} = m_{13} l_{13}^2/2$ is the polar moment of inertia of the half-circle attachment. In addition, the reaction force from the ground at the stance phase is given as the external force (the total mass of the mechanism) into the generalized coordinate $[x_{13}, y_{13}]$ in a numerical manner.

3.3 Theo Jansen mechanism

Finally, the mathematical model of the Theo Jansen mechanism is described in the same manner (Fig. 3). According to the vectors $\mathbf{q}$ with 39 elements including placements and attitude angles, the generalized coordinates are defined as follows:

$$\mathbf{q} = \left[\mathbf{q}_1^T, \mathbf{q}_2^T, \mathbf{q}_3^T, \mathbf{q}_4^T, \mathbf{q}_5^T, \mathbf{q}_6^T, \mathbf{q}_7^T, \mathbf{q}_8^T, \mathbf{q}_9^T, \mathbf{q}_{10}^T, \mathbf{q}_{11}^T, \mathbf{q}_{12}^T, \mathbf{q}_{13}^T\right]^T. \tag{23}$$

Although the original Theo Jansen mechanism is known as the system with 11 links, in this comparative analysis, an attachment with the ground and an extension link of the end-effector for normalization of the stride length and the total size against the driving link size are introduced as well as the previous section. Therefore, 39 $(= 13 \times 3)$ elements were obtained in the generalized coordinates in the present analysis.

A set of kinematic constraint equations $\mathbf{\Phi}$ is given by Eq. (3). The first 38 elements of the column matrix $\mathbf{\Phi}^K(\mathbf{q})$ are derived from kinematic constraint equations. The last element $\mathbf{\Phi}^D(\mathbf{q}, t)$ is derived by the driving constraint equation, the equation of kinematic constraints

and the driving constraint as shown below:

$$\boldsymbol{\Phi}(\mathbf{q},t)=\begin{bmatrix} x_1-l_1\cos\theta_1 \\ y_1-l_1\sin\theta_1 \\ x_2-l_2\cos\theta_2-x_1-l_1\cos\theta_1 \\ y_2-l_2\sin\theta_2-y_1-l_1\sin\theta_1 \\ x_3+l_3\cos\theta_3-x_2-l_2\cos\theta_2 \\ y_3+l_3\sin\theta_3-y_2-l_2\sin\theta_2 \\ x_3-l_3\cos\theta_3-a \\ y_3-l_3\sin\theta_3 \\ x_5+l_5\cos\theta_5-x_4+l_4\cos\theta_4 \\ y_5+l_5\sin\theta_5-y_4+l_4\sin\theta_4 \\ x_7-l_7\cos\theta_7-x_6+l_6\cos\theta_6 \\ y_7-l_7\sin\theta_7-y_6+l_6\sin\theta_6 \\ x_9+l_9\cos\theta_9-x_8+l_8\cos\theta_8 \\ y_9+l_9\sin\theta_9-y_8+l_8\sin\theta_8 \\ x_{11}-l_{11}\cos\theta_{11}-x_{10}+l_{10}\cos\theta_{10} \\ y_{11}-l_{11}\sin\theta_{11}-y_{10}+l_{10}\sin\theta_{10} \\ x_{12}-l_{12}\cos\theta_{12}-x_{10}+(l_{10}+2l_{12})\cos\theta_{10} \\ y_{12}-l_{12}\sin\theta_{12}-y_{10}+(l_{10}+2l_{12})\sin\theta_{10} \\ x_6+l_6\cos\theta_6-x_1-l_1\cos\theta_1 \\ y_6+l_6\sin\theta_6-y_1-l_1\sin\theta_1 \\ x_4+l_4\cos\theta_4-x_2-l_2\cos\theta_2 \\ y_4+l_4\sin\theta_4-y_2-l_2\sin\theta_2 \\ x_5-l_5\cos\theta_5 \\ y_5-l_5\sin\theta_5 \\ x_7+l_7\cos\theta_7 \\ y_7+l_7\sin\theta_7 \\ x_8+l_8\cos\theta_8-x_4+l_4\cos\theta_4 \\ y_8+l_8\sin\theta_8-y_4+l_4\sin\theta_4 \\ x_9-l_9\cos\theta_9-x_6+l_6\cos\theta_6 \\ y_9-l_9\sin\theta_9-y_6+l_6\sin\theta_6 \\ x_{10}+l_{10}\cos\theta_{10}-x_6+l_6\cos\theta_6 \\ y_{10}+l_{10}\sin\theta_{10}-y_6+l_6\sin\theta_6 \\ x_{11}+l_{11}\cos\theta_{11}-x_8+l_8\cos\theta_8 \\ y_{11}+l_{11}\sin\theta_{11}-y_8+l_8\sin\theta_8 \\ \theta_{12}-\theta_{10} \\ x_{13}-l_{13}\cos\theta_{13}-x_{12}+l_{12}\cos\theta_{12} \\ y_{13}-l_{13}\sin\theta_{13}-y_{12}+l_{12}\sin\theta_{12} \\ \theta_{13}-\theta_{12} \\ \theta_1-\omega t \end{bmatrix}_{39\times 1}=\mathbf{0}, \tag{24}$$

where l_1 to l_{13} are link lengths, t is time, and ω is the angular velocity of the crankshaft in the mechanism. Table 3 lists a set of parameter values of the Theo Jansen mechanism

Table 3 Parameters of link length and mass in the Theo Jansen mechanism

Parameter	Sides	Length ($\times 10^{-3}$ m)	Mass ($\times 10^{-3}$ kg)
l_1	O_1A	50.0	25.00
l_2	AB	200.0	100.00
l_3	O_2B	137.5	68.75
l_4	BC	200.0	100.00
l_5	O_2C	147.5	73.75
l_6	AD	200.0	100.00
l_7	O_2D	137.5	68.75
l_8	CE	142.5	71.25
l_9	DE	145.0	72.50
l_{10}	DF	140.0	70.00
l_{11}	EF	200.0	100.00
l_{12}	FG	40.0	20.00
l_{13}	G	1.0	0.5
a	O_1O_2	143.0	–

with additional two links for the grounding condition. Parameters are normalized as in the previous sections.

Therefore, the Jacobian matrix $\mathbf{\Phi}_q$ is obtained as

$$\mathbf{\Phi}_q = \left[\frac{\partial \mathbf{\Phi}(\mathbf{q}, t)}{\partial \mathbf{q}} \right]_{39\times 39}, \tag{25}$$

which allows us to investigate placement, velocity, and acceleration analyses kinematically.

The forward dynamics analysis introduces the mass matrix $\mathbf{M}$ (39×39), and the generalized external force vector $\mathbf{Q}^A$ (39×1) are described as follows:

$$\mathbf{M} = \mathrm{diag}(\mathbf{M}_1, \mathbf{M}_2, \ldots, \mathbf{M}_{13}), \tag{26}$$

$$\left\{ \mathbf{M}_i = [m_i, m_i, J_i]^T \;\middle|\; i = 1, \ldots, 13 \right\}, \tag{27}$$

$$\mathbf{Q}^A = \left[\mathbf{Q}_1^{A^T}, \mathbf{Q}_2^{A^T}, \ldots, \mathbf{Q}_{13}^{A^T} \right]^T, \tag{28}$$

$$\left\{ \mathbf{Q}_i^A = [0, -m_i g, 0]^T \;\middle|\; i = 1, \ldots, 13 \right\}, \tag{29}$$

where m_i is the mass of the rigid linkage to point i, $J_i = m_i l_i^2/3$ ($i = 1, \ldots, 12$) is the polar moment of inertia of the rigid linkage to point i, and g is the gravitational acceleration, and $J_{13} = m_{13} l_{13}^2/2$ is the polar moment of inertia of the half-circle attachment. In addition, the reaction force from the ground at the stance phase is given as the external force (the total mass of the mechanism) into the generalized coordinate $[x_{13}, y_{13}]$ in a numerical manner.

4 Characteristic analyses

According to the MBD descriptions in the above sections, characteristic analyses can be treated numerically, which allows for investigation of the temporal evolution of the placement, posture, velocity, acceleration, and torque in every joint, for elucidation of essential

Table 4 Parameters in the numerical simulation

Parameter	Description	Value
g	Gravitational acceleration	9.81 m/s^2
ω	Input angular velocity	2π rad/s (60 rpm)
α	Baumgarte parameter α	10
β	Baumgarte parameter β	$\sqrt{2\alpha}$
t	Time	$0 \leq t \leq 4$ s
dt	Time step	1.0×10^{-3} s
–	Solutions of ODE	Euler's method

differences between the three walking mechanisms. As for the limitation, the following analyses were calculated with effects of inertia of links with individual mass, the gravity at every moment, and the reaction force from the ground at the stance phase (the details are described in Sect. 5), yet the calculation did not include forces and torques that may arise from actual locomotion in the horizontal axis. In other words, it is the analysis of the ideal treadmill condition.

In the following sections, the MATLAB-based numerical simulation was used with the combinations of the Euler method with the time step of 1.0×10^{-3} s, as shown in Table 4. For comparison, parameters in Tables 1, 2, and 3 were normalized by rescaling the individual link lengths and the link weights, so that the crankshaft (driving link) radius is 0.1 m, the movement length at individual stance phase is 0.45 m, and the total weight is 0.87 kg. The constant angular velocity $\omega = 2\pi$ rad/s (60 rpm) was commonly given to the crankshaft rotation, and the Baumgarte stabilization method with parameters $\alpha = 10$ and $\beta = \sqrt{2\alpha}$ for maintaining stability in the MSD [62], for minimizing the accumulated error in numerical simulation to obtain the accurate solution. In placement, acceleration and torque analyses, the end effector (toe) was analyzed by using the generalized placement of the grounding link, as the half-circle attachment in Figs. 1, 2, and 3. According to the definition, the end-effector placement $D = [D_x, D_y]$ of the Chebyshev linkage is placed at the center of mass of the sixth link $[x_6, y_6]$, the end-effector placement of the Klann mechanism $E = [E_x, E_y]$ is calculated by the center of the 13th link $[x_{13}, y_{13}]$ and the end-effector placement of the Theo Jansen mechanism $G = [G_x, G_y]$ is the center of the 13th link $[x_{13}, y_{13}]$.

Table 5 showed representative factors obtained from the numerical analyses, which were calculated as the average from repetitive cycles at $t \in [0, 4]$ except unstable periods, in particular at the beginning for $t \in [0, 0.5]$.

4.1 Placements and postures

Placements and postures of the three mechanisms were measured under the normalized condition. Figures 4(a), 5(a), and 6(a) show the results of Chebyshev linkage, Klann mechanism, and Theo Jansen mechanism, respectively. The input force was given as the circular trajectory with the constant angular velocity ω shown as the circle at the origin in the figure, and the force was transferred to the end-effector (toe), which drew individual trajectory.

As shown in Table 5, the Klann had a maximum trajectory height of 0.36 m, and the Chebyshev and Theo Jansen mechanisms had similar trajectory heights. In the capability of lifting, which was defined as the ratio of the trajectory height to the mechanism height including movements, the Klann mechanism exhibited the maximum value of 52.17 % suitable for obstacle avoidance, and Theo Jansen mechanism showed the minimum of 8.05 %, which suggests less-energy consumption when in lifting motion.

Table 5 Results of characteristic analyses

Factor	Chebyshev	Klann	Theo Jansen
Height with movements [m]	**0.80**	**0.69**	**0.87**
(Highest placement [m])	(0.44)	(0.22)	(0.26)
(Lowest placement [m])	(−0.36)	(−0.47)	(−0.61)
Trajectory height [m]	**0.09**	**0.36**	**0.07**
(Maximum height of the leg [m])	(−0.27)	(−0.14)	(−0.54)
(Minimum height of the leg [m])	(−0.36)	(−0.50)	(−0.61)
Capability of lifting [%]	**11.25**	**52.17**	**8.05**
Average velocity [m/s]	**0.95**	**1.43**	**0.93**
(Maximum velocity [m/s])	(2.72)	(3.15)	(2.08)
(Minimum velocity [m/s])	(0.22)	(0.15)	(0.03)
#Local maxima of velocity change	**2**	**3**	**2**
Va [m/s]	2.72	3.15	1.02
(t^*)	($t = 0.507$)	($t = 0.074$)	($t = 0.081$)
Vb [m/s]	0.86	2.24	2.08
	($t = 0.996$)	($t = 0.378$)	($t = 0.546$)
Vc [m/s]	–	1.62	–
	–	($t = 0.815$)	–
Average acceleration [m/s^2]	**7.96**	**14.73**	**6.61**
(Maximum acceleration [m/s^2])	(23.17)	(32.24)	(15.17)
(Minimum acceleration [m/s^2])	(0.08)	(0.59)	(0.33)
#Local maxima of acceleration change	**2**	**4**	**3**
Aa [m/s^2]	23.17	22.74	12.76
(t^*)	($t = 0.445$)	($t = 0.237$)	($t = 0.388$)
Ab [m/s^2]	23.41	24.21	13.85
	($t = 0.571$)	($t = 0.443$)	($t = 0.497$)
Ac [m/s^2]	–	5.15	15.17
	–	($t = 0.702$)	($t = 0.630$)
Ad [m/s^2]	–	32.24	–
	–	($t = 0.945$)	–
Average absolute torque [Nm]	**0.84**	**0.52**	**0.23**
(Maximum torque [Nm])	(3.87)	(2.73)	(0.80)
(Minimum torque [Nm])	(−4.11)	(−1.21)	(−0.68)
#Local maxima of torque change	**2**	**4**	**2**
Ta [Nm]	0.21	0.19	0.80
(t^*)	($t = 0.025$)	($t = 0.141$)	($t = 0.499$)
Tb [Nm]	3.87	2.73	0.10
	($t = 0.557$)	($t = 0.424$)	($t = 0.971$)
Tc [Nm]	–	−0.24	–
	–	($t = 0.634$)	–
Td [Nm]	–	0.50	–
	–	($t = 0.893$)	–

* t represents time of the local maximum with respect to the single cycle (the period $T = 1$), which was calculated as the average time from multiple cycles; All the values were obtained as averages from repetitive cycles

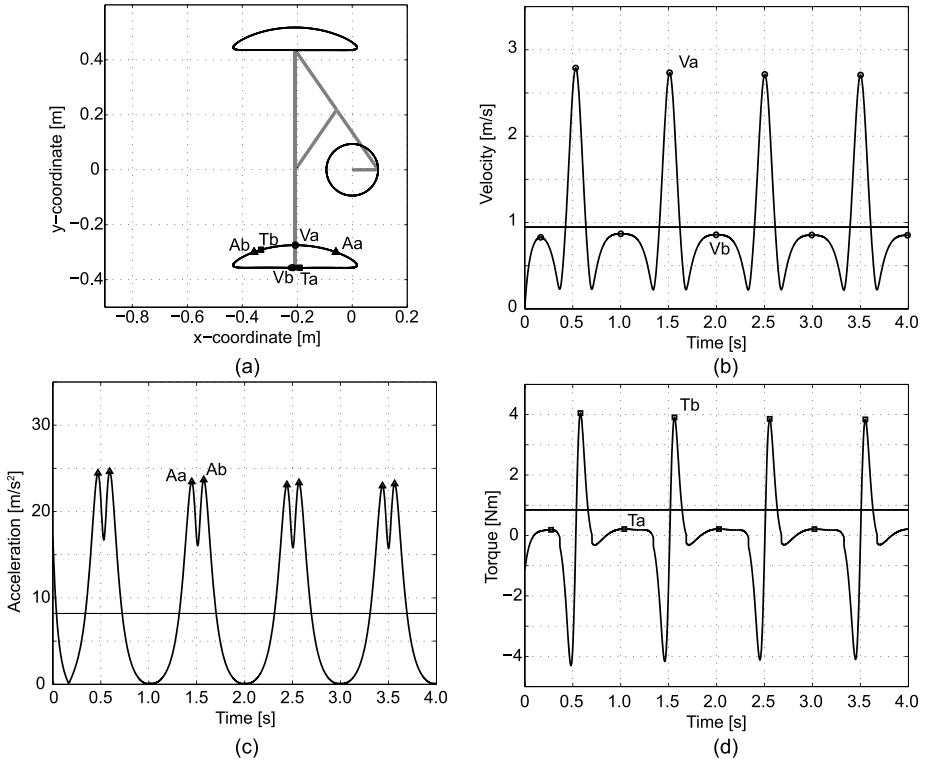

Fig. 4 Characteristic analyses including the end-effector placement $[D_x, D_y]$ (**a**), velocity $\sqrt{\dot{D_x}^2 + \dot{D_y}^2}$ (**b**), acceleration $\sqrt{\ddot{D_x}^2 + \ddot{D_y}^2}$ (**c**), and driving torque τ (**d**) of the Chebyshev linkage. *Horizontal lines* show the average of each set of values

4.2 Velocity and acceleration

Velocity and acceleration analyses of the three mechanisms are shown in Figs. 4(b)–(c), 5(b)–(c), and 6(b)–(c), respectively. For the sake of simplicity, the velocity vector $[\dot{x}, \dot{y}]$ and acceleration vector $[\ddot{x}, \ddot{y}]$ of the end-effector obtained from MBD analyses were respectively plotted by using the absolute values of $\sqrt{\dot{x}^2 + \dot{y}^2}$ and $\sqrt{\ddot{x}^2 + \ddot{y}^2}$ with respect to time.

According to the velocity analysis, the Klann mechanism had the highest average velocity of 1.43 m/s compared to the others, and it reached the maximum velocity of 3.15 m/s in the cycle, with respect to the shape of the trajectory (Fig. 5(a)). In the case of the Chebyshev linkage, the maximum velocity appeared at the highest point of the trajectory denoted as the positive peak Va (Fig. 4(a)), while the Klann Va appeared at the midpoint of the trajectory when in lifting motion before reaching the highest point, which was consistent with a positive peak of acceleration change Aa. The increase of the number of peaks denoted as Va, Vb, and Vc with respect to other mechanisms may help the maximization of the speed of lifting.

Comparing the shape of motion trajectories, the Chebyshev linkage and Theo Jansen mechanism did not exhibit a large difference, in comparison with the Klann mechanism, however, they differed in the temporal profile of velocity and acceleration. The Chebyshev

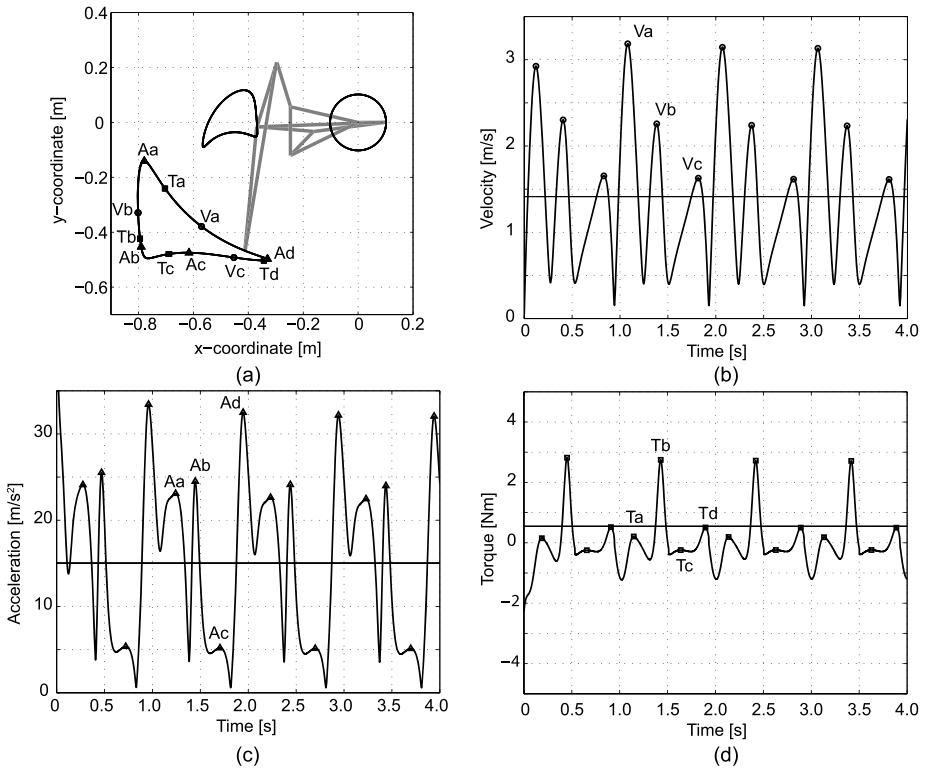

Fig. 5 Characteristic analyses including the end-effector placement $[E_x, E_y]$ (**a**), velocity $\sqrt{\dot{E_x}^2 + \dot{E_y}^2}$ (**b**), acceleration $\sqrt{\ddot{E_x}^2 + \ddot{E_y}^2}$ (**c**), and driving torque τ (**d**) of the Klann mechanism. *Horizontal lines* show the average of each set of values

linkage had a symmetric shape in up and down motion trajectories, while Theo Jansen mechanism provided a break of the symmetry.

Acceleration analysis showed that the Klann mechanism moves fast when the leg takes off from the ground and maximizes the acceleration just before touching the ground as shown in Fig. 5(c), and the acceleration vector may turn to the opposite direction for braking inertia force and preventing a large impact of the leg on the ground. Although the Chebyshev linkage (Fig. 4(b)–(c)) demonstrated profiles with a symmetric velocity and acceleration control, the Theo Jansen mechanism moved fast when the leg took off from the ground and maximized the acceleration just before touching the ground with less height of the leg, which provides a smooth grounding and contributes to the asymmetric acceleration control with three peaks Aa, Ab and Ac as shown in Table 5 and Fig. 6(c).

4.3 Torque analysis

Torque analyses of the three mechanisms are shown in Figs. 4(d), 5(d), and 6(d), respectively.

In the torque analysis as shown in Table 5, the Chebyshev linkage had maximum and minimum torques with a large amplitude in the interval $[3.87, -4.11]$ Nm, Klann mechanism had the torque range of $[2.73, -1.21]$ Nm, while for the Theo Jansen mechanism

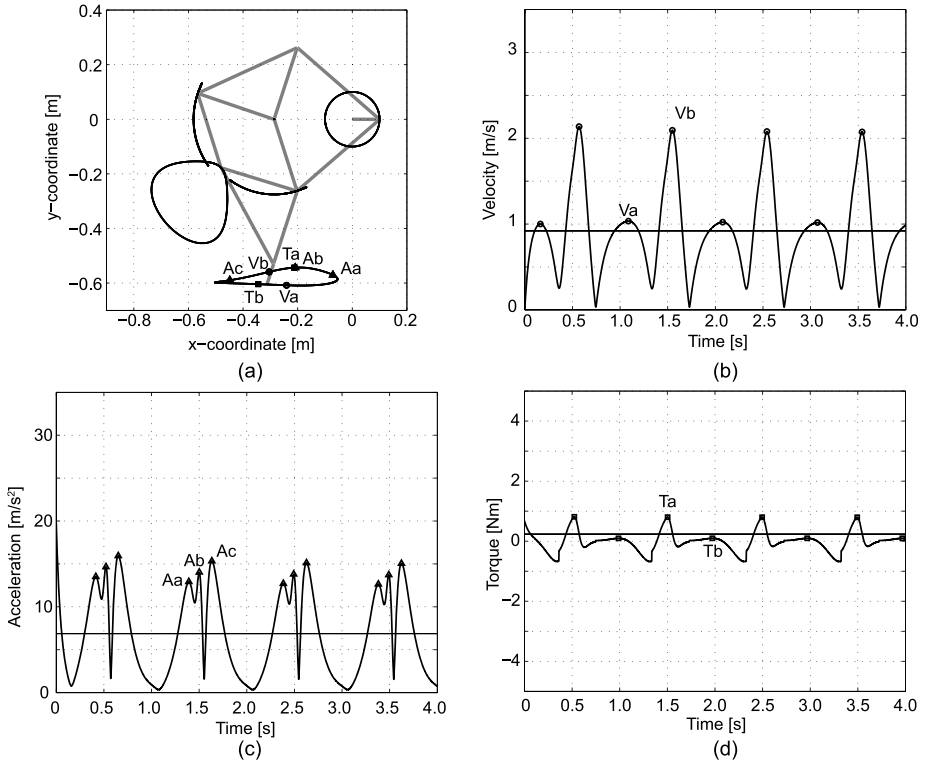

Fig. 6 Characteristic analyses including the end-effector placement $[G_x, G_y]$ (**a**), velocity $\sqrt{\dot{G_x}^2 + \dot{G_y}^2}$ (**b**), acceleration $\sqrt{\ddot{G_x}^2 + \ddot{G_y}^2}$ (**c**), and driving torque τ (**d**) of the Theo Jansen mechanism. *Horizontal lines* show the average of each set of values

torques were in a small range of [0.80, −0.68] Nm. The range will be mirrored in the energy consumption.

As a common property of the three closed-loop linkages, we observed a large peak point of the torque (T_b in the Chebyshev linkage and Klann mechanism, and T_a in the Theo Jansen mechanism) which was located at the swing phase before landing, and negative torque was observed at the stance phase, which contributes to separation of the swing and stance phases.

4.4 Acceleration on trajectory

Interestingly, the above characteristic analyses revealed a similarity of trajectory shapes of the Chebyshev linkage and Theo Jansen mechanism, while a dissimilarity appeared in the temporal evolutions of their acceleration and torque In the analysis of the detailed relationship between the trajectory and acceleration change, we investigated temporal evolutions of acceleration vectors of individual end-effector with respect to the trajectory position, such as $[\ddot{D}_x, \ddot{D}_y]$ in the Chebyshev linkage, $[\ddot{E}_x, \ddot{E}_y]$ in the Klann and $[\ddot{G}_x, \ddot{G}_y]$ in the Theo Jansen mechanisms, and then visualized their relationships as vector fields superimposed on individual trajectories as shown in Fig. 7.

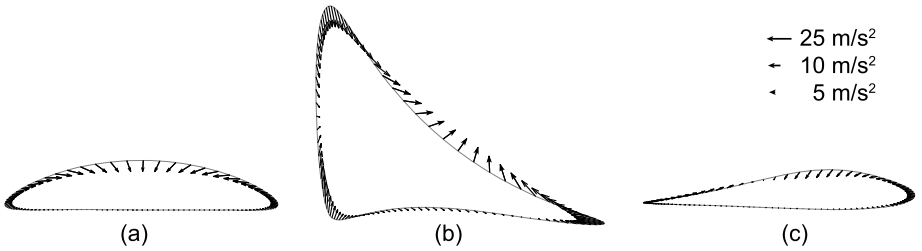

Fig. 7 Relationships between the leg's placement $[x, y]$ and the acceleration vector $[\ddot{x}, \ddot{y}]$ by using the vector field on the trajectory. The Chebyshev linkage (**a**), the Klann mechanism (**b**), and the Theo Jansen mechanism (**c**) were shown on the same scale

The length of each vector in Fig. 7 represents the absolute acceleration $\sqrt{\ddot{x}^2 + \ddot{y}^2}$ in temporal evolutions of Figs. 4(c), 5(c), and 6(c). The amount of the acceleration, i.e., the force generation, changes depending on the position of the trajectory to realize the fine tuning motion. Consistently, this superimposed image exhibited a symmetric pattern in the Chebyshev linkage, representing the same amount of force generated in the leg movement of lifting up and down at the swing phase. The characteristic acceleration peak at the top of the trajectory in the Klann mechanism maximizes the force generation just before falling down and changes the direction of force for braking the speed of the leg before touching the ground, and a similar vector rotation phenomenon appeared in the Theo Jansen mechanism, which works for a less-fluctuation landing. It is because the vectors in the latter part of the swing phase clearly fit the trajectory's tangential line. This is a clear evidence of how the Theo Jansen mechanism smoothly behaves in locomotion.

By extending the analysis to focus on the curvature property, the swing and stance phases were divided in the next section as the common criterion in the case of the closed-loop mechanism. This allows for the preparation of the detail analysis of energy consumption, thus providing further fair comparisons with walking machines in past studies.

5 Phases and duty factors

In order to detect walking phases in the three closed-loop mechanisms, the stance and swing phases can be divided by using the curvature property. The original curvature is defined as

$$\kappa(t) = \frac{\dot{x}\ddot{y} - \ddot{x}\dot{y}}{(\dot{x}^2 + \dot{y}^2)^{\frac{3}{2}}}, \tag{30}$$

where x and y are placements of the end-effector. For practical use as the criterion to determine edges of the stride length at the stance phase, we introduced the normalized curvature $\hat{\kappa}$ as

$$\hat{\kappa}(t) = \kappa(t)/\bar{\kappa}, \qquad \bar{\kappa} = \frac{1}{N}\sum_{t=t_0}^{t_1} \kappa(t), \tag{31}$$

where $T = [t_0, t_1]$ is the single cycle and N denotes the number of samples in the cycle. The first and second order derivatives in the equation were obtained by using the approxi-

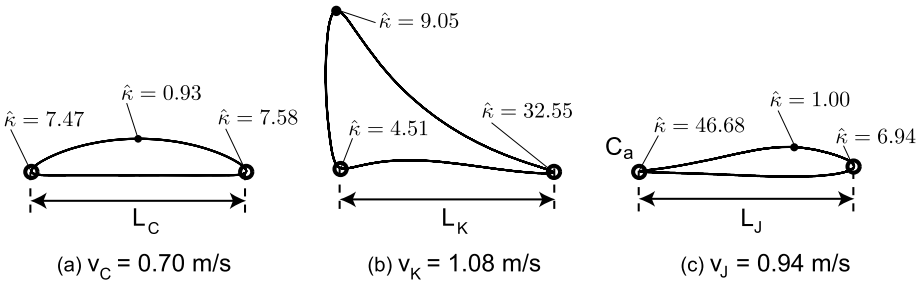

Fig. 8 Representative curvature peaks of the Chebyshev linkage (**a**), the Klann mechanism (**b**), and the Theo Jansen mechanism (**c**). The properties were required to determine the common stride length $L_C = L_K = L_J = 0.45$ m. The normalized curvature $\hat{\kappa}$ was calculated by Eq. (31) for a sample of $N = 1000$ observations. The high curvature points $\hat{\kappa} > 0.5$ were obtained as the average from the latter three cycles in the period $[1, 4]$ s in the numerical simulation, and they were plotted at the same individual points. The *points* used for the definition of the stance phase, i.e., start and end points of the stride length, were selected in a heuristic way by human inspection. The *open* and *closed circles* respectively represent points eligible for the decision of the stance phase and other ineligible points

mate derivative function based on the difference of neighboring points. As shown in Fig. 8, curvature peaks were found at moments when the leg is leaving and touching the ground, and then the representative two points were commonly used for the definition of the stance phase to determine the start and end points of the stride length. By using this criterion, the pure circle trajectory takes $\hat{\kappa} = 1$ at every point, and an ellipse with the ratio of 2 to 1 takes 2 at the higher peak point independent the radius.

In fact, we applied this formulation numerically to data under the assumption that neighboring points are smoothly interpolated, and then it matches the start and end points practically as shown in Fig. 8. In the viewpoint of the analytic solution of the trajectory curvature, especially on the Theo Jansen mechanism, the curvature, i.e., a function of differentials, does not exactly determine the turning points appearing in the numerical solution because there exists a zero-length loop at the point Ca in Fig. 8(c) analytically, which implies that the Theo Jansen mechanism's trajectory is a shrinkage of the figure-eight shape as recently revealed by Komoda and Wagatsuma [37].

In these mechanisms, the duty factor is consistently defined as:

$$D_i = \frac{t_i}{T} \quad (i = 1, \ldots, k), \tag{32}$$

where T is a walking cycle, t_i is the stance phase time, and k is the number of legs. Here periods $[t_c^{sw0}, t_c^{sw1}]$ and $[t_c^{st0}, t_c^{st1}]$ denote the swing and stance phases of the Chebyshev linkage; periods $[t_k^{sw0}, t_k^{sw1}]$ and $[t_k^{st0}, t_k^{st1}]$ denote the swing and stance phases of the Klann mechanism; and periods $[t_t^{sw0}, t_t^{sw1}]$ and $[t_t^{st0}, t_t^{st1}]$ denote the swing and stance phases of the Theo Jansen mechanism.

According to the definition, the Chebyshev linkage's duty factor was 0.66, the Klann mechanism's duty factor was 0.42, and the Theo Jansen mechanism's duty factor was 0.61 as shown in Fig. 9. In accordance with the investigation by McGhee [39], walking behaviors have duty factors greater than 0.5 and running behaviors have duty factors less than 0.5. Thus, the Chebyshev linkage and the Theo Jansen mechanism corresponded to walking behaviors, while the Klann mechanism exceeded this level, and so is more representative of running behavior.

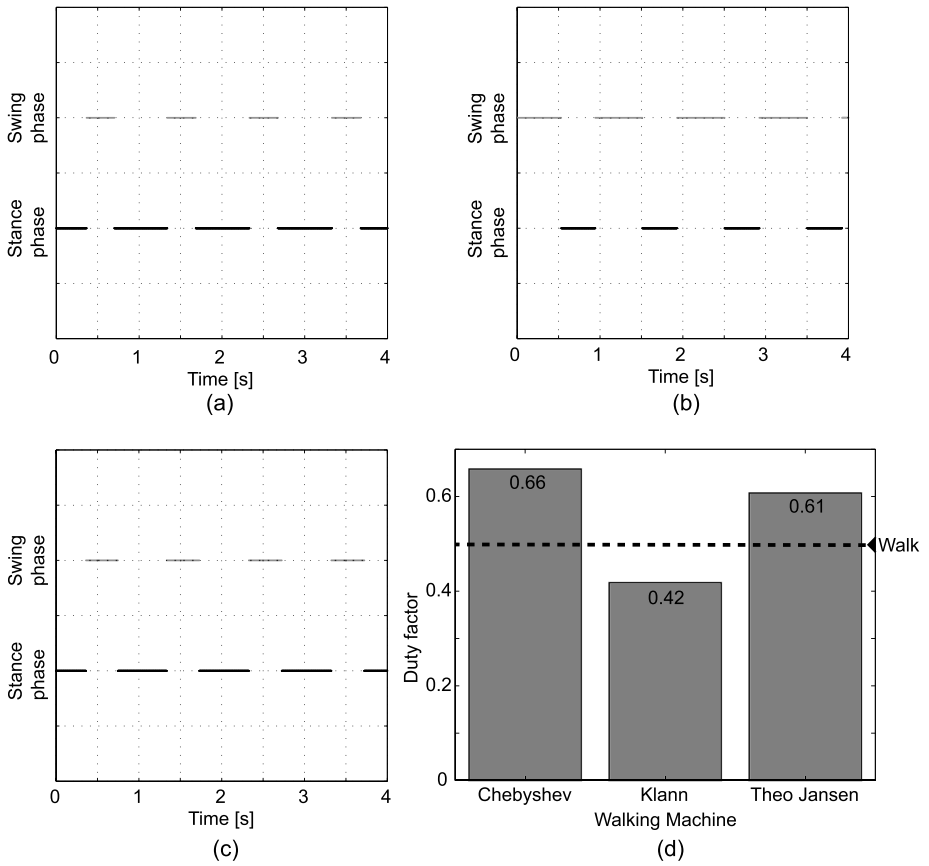

Fig. 9 Phase analysis of the Chebyshev linkage (**a**), the Klann mechanism (**b**), and the Theo Jansen mechanism (**c**)

6 Power and energy

6.1 Power consumption

Mechanical power is considered to be transmitted from the crankshaft input to the individual joints of linkages, and finally reaches the end-effector where the mechanical output of motor represents the power of the crankshaft. Considering the relationship between the driving torque of motor τ and the angular velocity ω, the power is the product of τ and ω as follows:

$$P = \tau\omega. \tag{33}$$

Table 6 shows representative factors obtained from the numerical analyses, which were calculated as averages from repetitive cycles for $t \in [0, 4]$ except for unstable periods, in particular at the beginning when $t \in [0, 0.5]$.

Power consumptions are obtained from the multiplication of the driving torque τ and the angular velocity ω, which was set constant in this analysis, as defined in Eq. (33),

Table 6 Results of power consumption

Factor	Chebyshev	Klann	Theo Jansen
Average absolute power (Type 1) [W]	**5.30**	**3.29**	**1.44**
Average positive power (Type 2) [W]	**3.96**	**4.70**	**1.25**
(Maximum power [W])	(24.31)	(17.13)	(5.03)
(Minimum power [W])	(−25.94)	(−7.61)	(−4.27)
#Peaks of power change	**4**	**8**	**5**
Pa [W]	1.33	−7.61	−4.27
(t^*)	($t = 0.025$)	($t = 0.013$)	($t = 0.312$)
Pb [W]	−25.94	1.22	5.01
	($t = 0.456$)	($t = 0.141$)	($t = 0.499$)
Pc [W]	24.31	−3.43	−1.11
	($t = 0.557$)	($t = 0.308$)	($t = 0.610$)
Pd [W]	−1.93	17.13	0.14
	($t = 0.708$)	($t = 0.424$)	($t = 0.726$)
Pe [W]	–	−2.43	0.60
	–	($t = 0.517$)	($t = 0.971$)
Pf [W]	–	−1.50	–
	–	($t = 0.634$)	–
Pg [W]	–	−1.83	–
	–	($t = 0.740$)	–
Ph [W]	–	3.15	–
	–	($t = 0.893$)	–

* t represents time of the peak with respect to the single cycle (the period $T = 1$), which was calculated as the average time from multiple cycles; All the values were obtained as averages from repetitive cycles

and therefore the temporal profiles of results in Sect. 4.3 were consistent with results in Fig. 10(a)–(c).

When comparing these three different linkages, the following common properties were clearly demonstrated: (i) positive power is generated when a leg is swinging in the air and moving quickly, and (ii) negative power is generated when a leg is on the ground at the stance phase. These common properties similarly appear in human behaviors such as walking and running. As is discussed in the next section in detail, the energy consumption is mainly based on the summation of the power consumption in a specific period, and how much power is needed depends on whether the system has energy storage capability when it takes negative powers transmitted to the driving link. The conventional definition requires the summation of the absolute power consumption ignoring the negativity, called 'Type 1' [55], while the summation of the power consumption only if it is positive is called 'Type 2' [50, 52]. Depending on the type of an animal, except small size insects, biological mechanisms potentially have a capability to store elastic strain energy in muscle and other tissues under ideal conditions [4, 5], and robots with elastic materials were designed to maximize the capability [11, 12]. The details will be discussed in Sect. 8.

In the analyses, we simply used Type 1 energy consumption in the next section according to traditional studies [55]. As a reference, a comparison of power consumptions based on Type 1 and Type 2 is shown in Fig. 10(d).

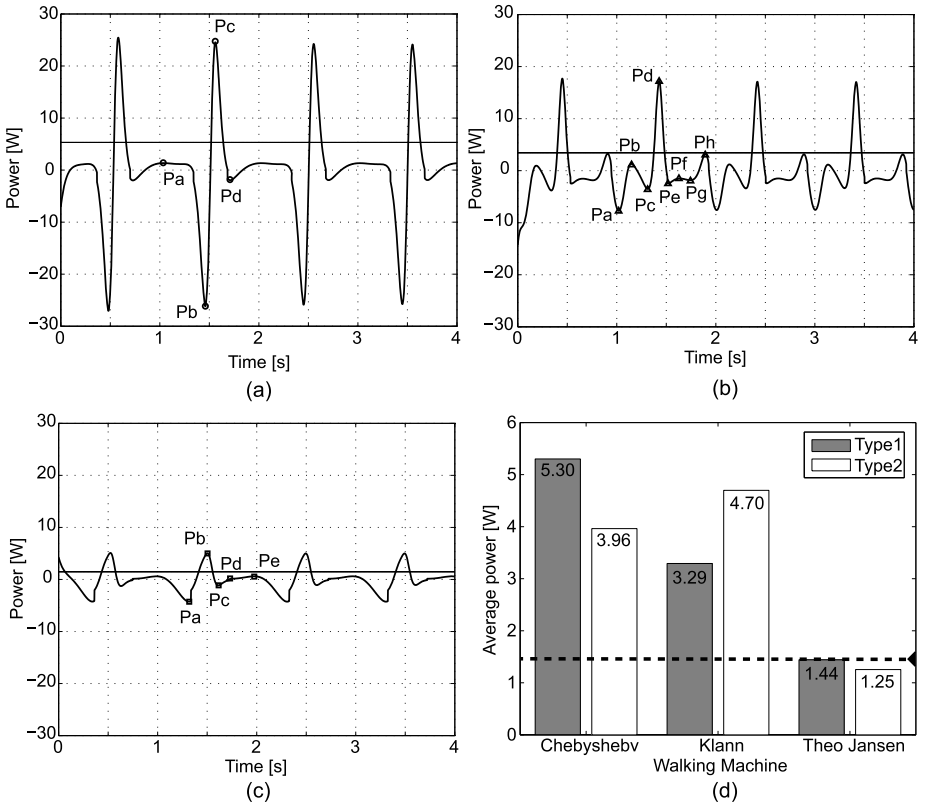

Fig. 10 Power analyses of the Chebyshev linkage (**a**), the Klann mechanism (**b**), and the Theo Jansen mechanism (**c**). Average power was calculated in Type 1 and Type 2 definitions (in text) as the average value in a cycle (**d**). Type 2 is larger than Type 1 and represents a sharp peak during the positive period without any large negative peak

6.2 Energy consumption

Energy consumption of the crankshaft is evaluated by the integral of the absolute value of the driving torque of the motor and the angular velocity of the crankshaft and described mathematically if thermal dissipation in the system is assumed to be zero in the ideal case as

$$E = \int_{t_0}^{t_1} |\tau\omega|\, dt, \tag{34}$$

where t_i is the time [27, 49–52]. This measurement represents output of the actuators and it does not include the joints' energy and transmission efficiency of the mechanism, as well as the definition of Schiehlen [55].

Figure 11 shows the results of the temporal evolution of individual energy consumptions E of the Chebyshev linkage, the Klann mechanism, and the Theo Jansen mechanism. As defined in Eq. (32), the Chebyshev linkage has the swing phase $[t_c^{sw0}, t_c^{sw1}]$ and the stance

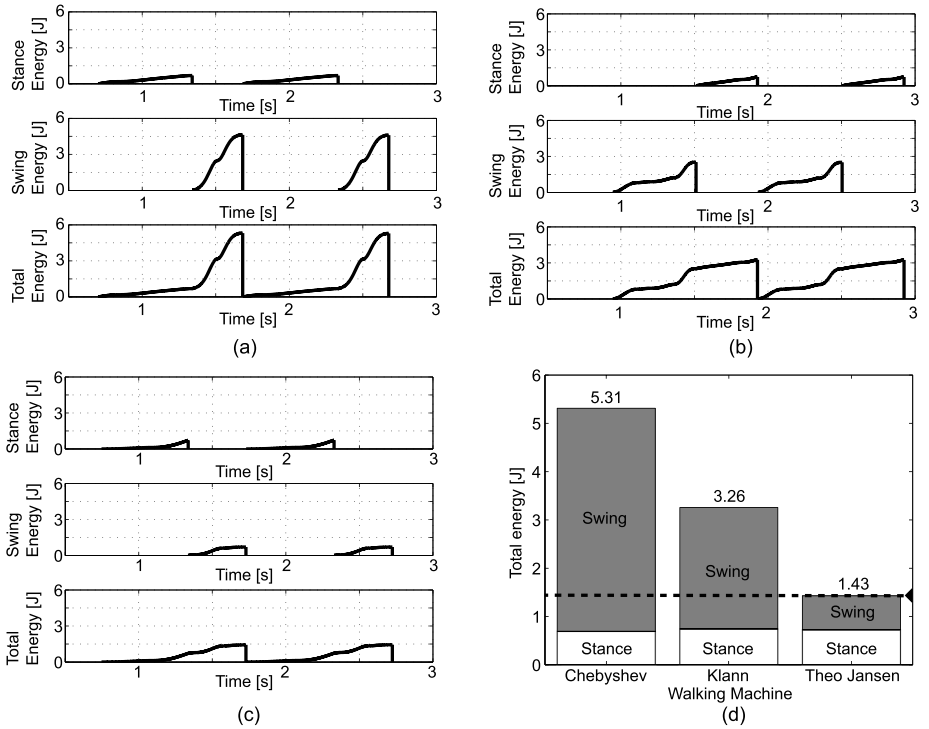

Fig. 11 Cumulative plots of energy consumptions of the Chebyshev linkage (**a**), the Klann mechanism (**b**), and the Theo Jansen mechanism (**c**). Total energy consumptions E_c, E_k, and E_t are shown in (**d**)

phase $[t_c^{st0}, t_c^{st1}]$; the Klann mechanism has the swing phase $[t_k^{sw0}, t_k^{sw1}]$ and the stance phase $[t_k^{st0}, t_k^{st1}]$; and the Theo Jansen mechanism has the swing phase $[t_t^{sw0}, t_t^{sw1}]$ and the stance phase $[t_t^{st0}, t_t^{st1}]$. Therefore, the energy consumption of the swing and stance phases of the Chebyshev linkage are respectively $E_c^{sw1} = \int_{t_c^{sw0}}^{t_c^{sw1}} |\tau\omega|\, dt$ and $E_c^{st1} = \int_{t_c^{st0}}^{t_c^{st1}} |\tau\omega|\, dt$, and then the total energy consumption is calculated as $E_c = E_c^{sw1} + E_c^{st1}$. In the cases of the Klann and Theo Jansen mechanisms, $E_k = E_k^{sw1} + E_k^{st1}$ and $E_t = E_t^{sw1} + E_t^{st1}$ were similarly obtained. As shown in Fig. 11(a), in the Chebyshev linkage, the energy consumptions of the swing and stance phases were $E_c^{sw1} = 4.62$ J and $E_c^{st1} = 0.69$ J, and the total energy consumption was $E_c = 5.31$ J.

In the Klann mechanism, the energy consumptions of the swing and stance phases were $E_k^{sw1} = 2.52$ J and $E_k^{st1} = 0.74$ J, and then the total energy consumption was $E_k = 3.26$ J (Fig. 11(b)). In the Theo Jansen mechanism, the energy consumptions of the swing and stance phases were $E_t^{sw1} = 0.71$ J and $E_t^{st1} = 0.72$ J, and then the total energy consumption was $E_t = 1.43$ J (Fig. 11(c)).

Thus, the three mechanisms consistently consume more energy in the stance phase, and the Theo Jansen mechanism consumes the least total energy when compared to the other two mechanisms, as summarized in Fig. 11(d), which scores 3.7 times better than Chebyshev and 2.3 times better than Klann. This result indicated that the Theo Jansen mechanism is the most effective walking mechanism of the three closed-loop linkages.

7 Specific resistance

For evaluating the energy efficacy in walking legged robots, the general criterion called 'specific resistance' was proposed by Gabrielli and von Kármán [23] as follows:

$$\epsilon = \frac{P}{mgv}, \tag{35}$$

where P is the output power, m is the total weight, and v is the walking speed [13]. This measure allows for the comparison of different locomotion machines with respect to the energetic performance.

For all three closed-loop mechanisms, as is consistent with the above sections, common properties were given as follows: the angular velocity of the crankshaft $\omega = 2\pi$ rad/s, the total weight $M_C = M_K = M_J = 0.87$ kg and the stride length $L_C = L_K = L_J = 0.45$ m.

The specific resistance of the Chebyshev linkage was obtained as $\epsilon = 1.42$ with the walking speed $v = 0.49$ m/s and the power $P = 3.04$ W. The Klann's specific resistance was $\epsilon = 0.91$ with $v = 0.45$ m/s and $P = 3.35$ W. In the case of the Theo Jansen mechanism, the specific resistance was $\epsilon = 0.31$ with $v = 0.46$ m/s and $P = 1.21$ W. As a consequence, the energy-efficacy of the Theo Jansen mechanism was the minimum for $\omega = 2\pi$ rad/s.

In further analysis, we investigated the specific resistances with respect to the walking speed, which can be modified by the angular velocity of the driving link. The result with angular velocities ranging in $[\pi/4, 10\pi]$ with the $\pi/4$ step is shown in Fig. 12, which demonstrates the monotonic increase with a consistent exponential property. When comparing these three mechanisms, the Theo Jansen mechanism demonstrated the minimum specific resistance value in the whole range of angular velocities $\omega \in [\pi/4, 10\pi]$. Interestingly, the Klann and Theo Jansen mechanisms had a similar profile with respect to the walking speed. For the same angular velocity $\omega = 10\pi$ rad/s, the Theo Jansen mechanism showed $\epsilon = 3.01$ and $v = 3.83$ m/s, while the Klann mechanism increased its walking speed to $v = 5.43$ m/s with $\epsilon = 6.74$, which means that the walking speed is 1.42 times greater and the specific resistance is 2.24 times greater than those of the Theo Jansen's. The Klann mechanism is good at increasing of the walking speed, accompanied with the increase of the specific resistance. In regard to the specific resistance, this result indicated that the Theo Jansen mechanism has the least energy consumption among the three mechanisms.

Figure 13 shows a log–log scale plot of the general evaluation of the mechanisms in comparison to other proposed walking machines in the literature, such as monopod, biped, quadruped, six-legged, and human walking and running. A famous hopping robot, Gregorio's ARL monopod I [24], which was a 15 kg planar one-legged robot, and an ARL monopod II [2], which was a 18 kg planar one-legged running robot with hip and leg compliance, were included, and their specific resistances were similar, $\epsilon \in [0.2, 11]$, to the three closed-loop mechanisms, even though the mechanism for the hopping movement was quite different from the controlled passive dynamic running strategy.

Cavagna and Kaneko [15] investigated how human walking and running requires energy in regards to the specific resistance. They measured the total mechanical energy in the variations of kinetic and potential energy in the body trunk while walking and running. The famous McGeer's gravity walker [38] represented the simplest passive walker with a weight of 3.5 kg and two legs, which walked smoothly using only the potential energy from its own gravity. The Cornell walker [18] was a 13 kg passive dynamic walker moving at 0.4 m/s with $\epsilon = 0.055$, and was composed of solid parts connected by joints. In the case of the Cornell three-dimensional passive walker [17], the 4.8 kg system was more complex than the other passive walkers, and it could reach a walking speed of 0.51 m/s with $\epsilon = 0.054$.

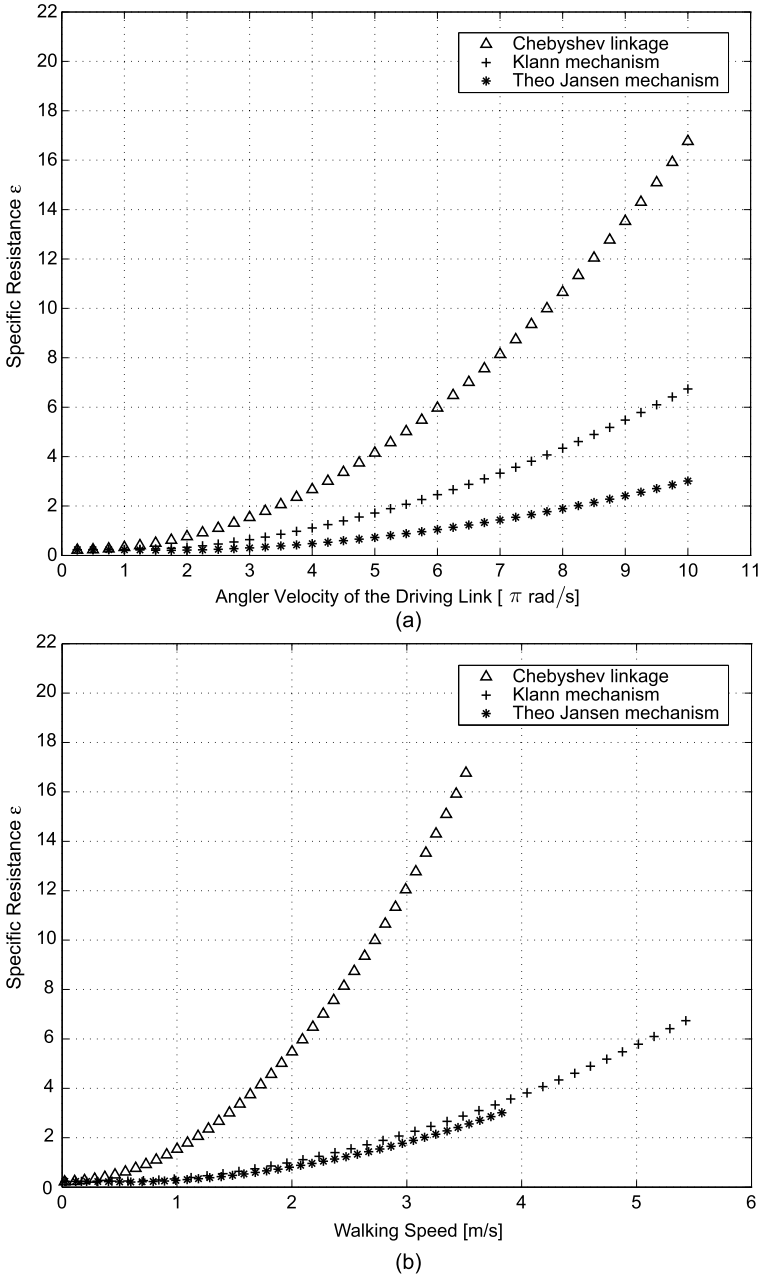

Fig. 12 Specific resistance analyses of the three closed-loop linkages with respect to the angular velocity ω [π rad/s] (a) and the walking speed v [m/s]

Although these passive dynamic walking machines have no electric actuator and controller, the system's interaction with the ground provides an efficient way of bipedal walking, which resembles human locomotion. Schiehlen [55] developed a bipedal locomotion system with

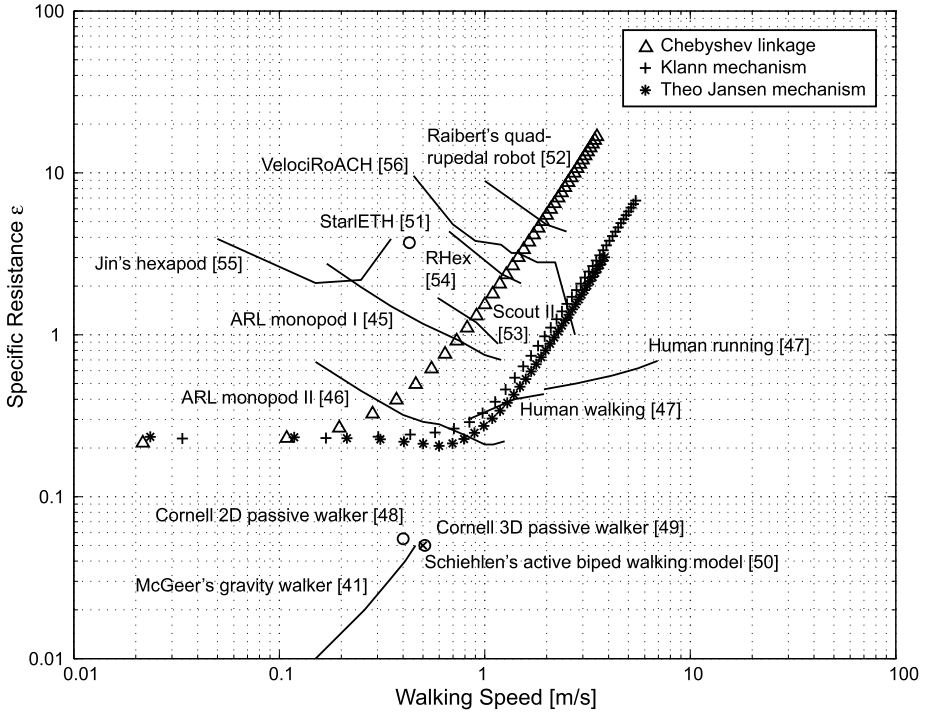

Fig. 13 Specific resistance of walking machines and humans

a weight of 20 kg in the form of the active biped walking model, in which the walking speed was about 0.5 m/s and the specific resistance $\epsilon = 0.05$. This model successfully reduced the energy consumption by using a method for energy efficient control in a biped walking machine.

StarlETH [28] proposed a 23 kg compliant quadrupedal robot, with a trotting gait walking at the speed of 0.43 m/s, when electric power equals 360 W. The robot was designed as a device with an adaptive torque control mechanism. Raibert's quadrupedal robot [48] was as heavy as 32 kg, and had multiple modes of running gaits-based legs moving in pairs: the trot, pace and bound locomotion. Scout II [63] was a 24 kg autonomous four-legged robot with only one actuator per compliant leg. This robot achieved a running speed of up to 1.2 m/s when it employed a bounding gait. RHex [14] was an autonomous hexapod with 8 kg power, which consisted of a single actuator per compliant leg. The robot generated gait patterns, including a tripod gait and a bounding gait. Jin's hexapod walking robot [33] weighted 5.26 kg, which was controlled autonomously by the torque distribution algorithm to minimize the system's energy cost. VelociRoACH [25] was a 30×10^{-3} kg hexapedal millirobot capable of running at 2.7 m/s. Its creators developed a new gait tuning method for millirobots, which was designed for finding stable limit cycles which minimized the amount of rotational energy in their systems.

As shown in Fig. 13, specific resistances of these walking machines were plotted using the same measures, and they were distributed around the properties of the human walking and running movements. Naturally, passive dynamic walking machines using potential energy based on gravity achieved locomotion with lower specific resistances than that of human walking and running, which was considered a typical biological locomotion system

with less energy consumption. This result indicated that the specific resistance increases in passive walking machines and human locomotion with respect to the walking speed, while it decreases in the cases of monopod, quadruped, and hexapod systems.

Interestingly, for the closed-loop mechanisms, the specific resistance presents a proportional increase with respect to the walking speed, which was not consistent with other multi-legged walking machines (including monopods) but was consistent with human walking and running. The minimum specific resistance of the Theo Jansen mechanism was close to that of human walking. While the monopod based on the air spring has a similar level, the closed-loop mechanism can reach this level by providing a smooth grounding to prevent loss of energy at the moment the leg touches the ground.

8 Discussion

8.1 Regeneration energy and inertia torques

In the analysis of the energy consumption in Sect. 6.2, we used an equation that is consistent with Schiehlen [55] in the form of Eq. (34), focusing on the absolute value of the work and ignoring the thermal dissipation. In principle, the energy consumption is formulated as follows [27, 49–52]:

$$E = \int_{t_0}^{t_1} f(\tau\omega)\, dt + \int_{t_0}^{t_1} \gamma \tau^2\, dt, \tag{36}$$

where f is a function to calculate the mechanical work from the torque τ and the angular velocity ω, and γ is the thermal dissipation constant.

As described in Table 7, the energy consumption depends on what type of actuator is used in the driving motor. In the present comparative study, we simply assumed the Type 1 energy consumption, corresponding to conditions with the slow movement based on conventional actuators. It is plausible for the Chebyshev linkage and the Theo Jansen mechanism because they showed duty factors to be in a walking mode. In the viewpoint that the Klann mechanism showed the duty factor as a running mode, it may have a potential to improve the energy consumption by adding the regeneration system when kicking the ground, such as a spring system. In the consideration that increasing the size of the Klann is not beneficial according to our characteristics analysis, it is difficult for the small-sized robot to introduce the regeneration system, similar to that of insects. Therefore, a comparison of closed-loop

Table 7 Types of the energy consumption depending on the actuator

Type	Positive work	Static work	Negative work	f
Type 1	+	+	+	$\lvert\tau\omega\rvert$[1]
Type 2	+	0	0	0 ($\tau\omega \leq 0$)[2]
Type 3	+	0	–	$\tau\omega$[3]

[1] Conventional actuators without brake [55]; muscles in slow motion

[2] Actuators with brake (or geared with a high reduction ratio); muscles of insects [51]

[3] Actuators with regeneration brake [6, 20, 57]; Coupling of muscles with the tendon in high speed movements [4, 5, 7]

linkages is considered to be validated enough. On the other hand, the ideal treadmill condition has the limitation in the dynamic aspect of the movement. For actual production of walking/running machines, forces and torques that may arise from actual locomotion, including friction and thermal dissipation in collision of the leg with the ground surface, are crucial for pre-investigation. In fact, the MBD-based approach allows us to extend such a further analysis.

In the recent trend of bio-inspired robots, the Type 3 energy consumption is a factor to improve the running speed drastically. The bio-inspired legged robot, MIT Cheetah, achieved 21 km/h (13 mph) as the highest mark in recent running machines [6, 20, 57], using a regenerative motor driver connecting its closed linkage legs. The evidence indicates that the same mechanism can commonly be introduced to closed-loop linkages. Another possible option of the energy regeneration of the energy is energy storage with passive compliance, which is obtained from spring and elastic materials [11]. The property of the energy storage is known in the artificial legs made of elastic materials, such as carbon fiber prostheses [65]. In this analysis, we used DAEs in the MBD analysis only with rigid bodies, which are treated by total differential equations, and the hybrid system composed of rigid bodies and elastic materials requires the extension of DAEs to involve calculations of a set of partial differential equations simultaneously, such as the finite element method.

8.2 Possible reduction of dimensions

A further possible discussion is the problem of dimensionality. Beside forward kinematics and inverse kinematics, kinematic synthesis is an important tool to explore the best dimensionality for the target system design [46, 47]. In regard to the target system in the present study, the inventor of the mechanism, Theo Jansen, practically treated a kinematic synthesis by using a heuristic approach based on the evolutionary algorithm such that 1500 sets were randomly generated in the design process, 100 sets were selected automatically with a cost function, and then the best one was chosen according to a human expert inspection [32].

According to basic principle of generalized coordinates in the MBD [59], we analyzed the target closed-loop system to assign local coordinates with individual links; however, the dimension reduction is possible if a set of components can be treated as one rigid body. For example, in this case, the triangle structure in the mechanism does not change its form except for parallel movements and rotations, which leads to a reduction of the number of equations. The downsizing of the Jacobian matrix contributes to a reduction of the computational cost and prevention of the accumulation error in numerical simulation, while if the downsizing protocol is not systematic, and is rather heuristic, it impairs the advantage of the generalized coordinate system in the MBD procedure. A recent topic on the dimension reduction is discussed in the field of differential geometry. The center manifold reduction has long been studied in the field [9, 45, 61, 64, 66], recently the Morse theory was highlighted [1, 21, 30, 41], and then applied to the dimension reduction for the investigation of bipedal walking models [44]. A working and plausible hypothesis on dimensions of biological mechanisms is that many degrees of freedom in the body kinematics are controlled by nervous systems to reduce the freedom by adding constraints with the purpose that the whole system provides the target behavior. This concept realizes in the MBD formulation in ways of increasing the ratio of driving constraints and introducing complex interactions between rigid bodies.

In contrast, increasing the number of degrees of freedom is also beneficial to provide multiple functional motions from the single mechanism. As we analyzed, the Theo Jansen mechanism has an optimal motion for walking to minimize the lifting height of the leg.

This property is simultaneously an advantage and disadvantage if flexible motions need to be considered. Recently Komoda and Wagatsuma [37] revealed that the Theo Jansen has a large expandability to provide multiple functional motions by releasing the fixed node of O_2 in Fig. 3 as the second movable node. The modified system provides other functional trajectories if O_1 and O_2 are synchronously moved in a specific phase relationship. This implies that unexpected and non-intuitive possibilities of the biological mechanism can be analyzed in the mechanical sense, providing a clue of how it can be utilized in a machine [16, 60].

9 Conclusions

In our results, the Chebyshev linkage, Klann and Theo Jansen mechanisms showed different properties in individual acceleration and torque temporal profiles, while they had consistent tendencies regarding total energy consumptions and energy-efficacies, which were proportional to the walking speed. The Theo Jansen mechanism was the best and the Klann mechanism was the worst in regard to the total energy consumption. Since the Klann mechanism was initially designed as a system to mimic insect motion, it needs to be built in a smaller size to be able to move with a limited energy, yet it quickly moves in a running mode with the highest locomotion speed, rather than others. The Theo Jansen is considered to be an extended version of the Chebyshev linkage due to similarities of basic velocity and acceleration profiles and the existence of additional peak points, and therefore in this comparison the Theo Jansen mechanism is an optimum solution as the linkage specialized for walking smoothly.

By using the MBD-based numerical analyses, this study newly revealed that the specific resistances of three linkages were proportional to their walking speeds, which is not consistent with walking machines in past studies like ARL monopod I and II, yet it is consistent with human walking and running. Our hypothesis was successfully proved based on the characteristic analyses of multibody dynamics.

As a similarity of biological and robotic evolutions [16, 60], our results imply that the Chebyshev linkage provides the simplest motion trajectory in the sense of fewer dimensions for achieving a function of walking, and in contrast the Theo Jansen mechanism realized a fine profile of force changes along the trajectory by using complex links, even though the dimensions are increased. Further properties will be discussed in a combined analysis with tools of kinematic synthesis [19, 46, 47].

Acknowledgements This research is partially supported by JSPS KAKENHI 22300081, 16H01616 and 26240032, the "Brain-IS Research Project" promoted in the Department of Brain Science and Engineering, Graduate School of Life Science and Systems Engineering, Kyushu Institute of Technology, the Matching Planner Program from Japan Science and Technology Agency, JST, the New Energy and Industrial Technology Development Organization (NEDO) "Next-generation Artificial Intelligence", the Council for Science, Technology and Innovation, "Cross-ministerial Strategic Innovation Promotion Program (SIP), Infrastructure Maintenance, Renovation, and Management" (funding agency: NEDO), and the MEXT Selected Program for Promoting Inter-University Collaborative Education in FY2012, "Joint Graduate School in Intelligent Car & Robotics Course."

The authors would like to extend their sincere appreciation to the inventor of the Strandbeests, Theo Jansen, for giving them an invaluable inspiration to work on this paper, when he came to Japan in the first time in 2009, seven years ago, and a brilliant motivation to carry the system to sophisticated mathematical approaches, enlarging the hidden potential to the maximum extent possible and contributing to an evolution of 'new forms of life' as he said.

References

1. Acar, E.U., Choset, H., Rizzi, A.A., Atkar, P.N., Hull, D.: Morse decompositions for coverage tasks. Int. J. Robot. Res. **21**(4), 331–344 (2002)
2. Ahmadi, M., Buehler, M.: The ARL monopod II running robot: control and energetics. In: Proceedings of 1999 IEEE International Conference on Robotics and Automation, vol. 3, pp. 1689–1694 (1999)
3. Alessandro, C., Delis, I., Nori, F., Panzeri, S., Berret, B.: Muscle synergies in neuroscience and robotics: from input-space to task-space perspectives. Front. Comput. Neurosci. **7**, 43 (2013). doi:10.3389/fncom.2013.00043
4. Alexander, R.M.: Tendon elasticity and muscle function. Comp. Biochem. Physiol., Part A **133**, 1001–1011 (2002)
5. Alexander, R.M., Bennet-Clark, H.C.: Storage of elastic strain energy in muscle and other tissues. Nature **265**(5590), 114–117 (1977)
6. Alexandre, T.: Improvement of the cheetah locomotion control. Master's Project, École polytechnique fédérale de Lausanne. http://biorob.epfl.ch/files/content/sites/biorob/files/users/183877/public/TuleuReport29012010.pdf (2010)
7. Bauer, F., Römer, U., Fidlin, A., Seemann, W.: Optimization of energy efficiency of walking bipedal robots by use of elastic couplings in the form of mechanical springs. Nonlinear Dyn. **83**(3), 1275–1301 (2016)
8. Baumgarte, J.: Stabilization of constraints and integrals of motion in dynamical systems. Comput. Methods Appl. Mech. Eng. **1**, 1–16 (1972)
9. Benner, P., Mehrmann, V., Sorensen, D.: Dimension Reduction of Large-Scale Systems. Springer, Berlin (2005)
10. Bernstein, S.N.: The Scientific Legacy of P.L. Chebyshev (1945)
11. Braun, D., Howard, M., Vijayakumar, S.: Exploiting variable stiffness in explosive movement tasks. In: Proceedings of Robotics: Science and Systems (2011). doi:10.15607/RSS.2011.VII.004
12. Braun, D., Howard, M., Vijayakumar, S.: Exploiting variable stiffness in explosive movement tasks. In: Robotics: Science and Systems VII, pp. 25–32. MIT Press, Cambridge (2012)
13. Buehler, M.: Dynamic locomotion with one, four and six-legged robots. J. Robotics Soc. Jpn. **20**(3), 237–242 (2002)
14. Campbell, D., Buehler, M.: Preliminary bounding experiments in a dynamic hexapod. In: Experimental Robotics, vol. VIII, pp. 612–621 (2003)
15. Cavagna, G.A., Kaneko, M.: Mechanical work and efficiency in level walking and running. J. Physiol. **268**, 467–481 (1977)
16. Cianchetti, M., Calisti, M., Margheri, L., Laschi, M.K.C.: Bioinspired locomotion and grasping in water: the soft eight-arm octopus robot. Bioinspir. Biomim. **10**(3), 035, 003 (2015)
17. Collins, S.H., Wisse, M., Ruina, A.: A three-dimensional passive-dynamic walking robot with two legs and knees. Int. J. Robot. Res. **20**, 607–615 (2001)
18. Collins, S., Ruina, A., Tedrake, R., Wisse, M.: Efficient bipedal robots based on passive-dynamic walkers. Science **307**, 1082–1085 (2005)
19. Coros, S., Beaudoin, P., Yin, K., van de Panne, M.: Synthesis of constrained walking skills. ACM Trans. Graph., Proc. Siggraph Asia **27**(5), 113 (2008)
20. DARPA: Darpa cheetah sets speed record for legged robots (2012). https://www.youtube.com/watch?v=d2D71CveQwo
21. Farley, D., Sabalka, L.: Discrete Morse theory and graph braid groups. Algebraic Geom. Topol. **5**, 1075–1109 (2005)
22. Flores, P., Machado, M., Seabra, E., da Silva, M.T.: A parametric study on the Baumgarte stabilization method for forward dynamics of constrained multibody systems. J. Comput. Nonlinear Dyn. **6**, 1–9 (2011)
23. Gabrielli, G., von Kármán, T.: What price speed? Specific power required for propulsion of vehicles. Mech. Eng. **72**, 775–781 (1950)
24. Gregorio, P., Ahmadi, M., Buehler, M.: Design, control, and energetics of an electrically actuated legged robot. IEEE Trans. Syst. Man Cybern., Part B, Cybern. **27**, 626–634 (1997)

25. Haldane, D.W., Peterson, K.C., Garcia Bermudez, F.L., Fearing, R.S.: Animal-inspired design and aerodynamic stabilization of a hexapedal millirobot. In: Proceedings of 2013 IEEE International Conference on Robotics and Automation (ICRA), pp. 3279–3286 (2013)
26. Haug, E.J.: Computer Aided Kinematics and Dynamics of Mechanical Systems: Basic Methods, vol. 1. Allyn and Bacon, Boston (1989)
27. Hirose, S., Kikuchi, H., Umetani, Y.: The standard circular gait of a quadruped walking vehicle. Adv. Robot. **1**(2), 143–164 (1986)
28. Hutter, M., Gehring, C., Bloesch, M., Hoepflinger, M., Siegwart, R.: Walking and running with StarlETH. In: Proceedings of the 6th International Symposium on Adaptive Motion of Animals and Machines (AMAM) (2013)
29. Ingram, A.J.: A new type of mechanical walking machine. Ph.D. thesis, Department of Mechanical and Industrial Engineering Technology, University of Johannesburg, Johannesburg, South Africa (2006)
30. Ivancevic, V., Pearce, C.: Hamiltonian dynamics and Morse topology of humanoid robots. Glob. J. Math. Math. Sci. **1**(1), 9–18 (2005)
31. Jansen, T.: Theo Jansen: The Great Pretender. Nai010 Publishers, Rotterdam (2007)
32. Jansen, T.: Strandbeest. http://www.strandbeest.com/
33. Jin, B., Chen, C., Li, W.: Power consumption optimization for a hexapod walking robot. J. Intell. Robot. Syst. **71**, 195–209 (2013)
34. Kane, T.R., Levinson, D.A.: Dynamics, Theory and Applications. McGraw-Hill, New York (1985)
35. Klann, J.: Walking device, Nov. 12, 2002. US Patent 6478314
36. Komoda, K., Wagatsuma, H.: Singular configurations analyses of the modifiable Theo Jansen-like mechanism by focusing on the Jacobian determinant—a finding limitations to exceed normal joint range of motion. In: Proceedings of 2014 IEEE/ASME International Conference on Advanced Intelligent Mechatronics (AIM), pp. 76–81 (2014)
37. Komoda, K., Wagatsuma, H.: A determinant analysis to detect the singularity of the extended Theo Jansen mechanism in the phase-rotation-amplitude parameter space. J. Comput. Sci. Syst. Biol. **9**(1), 10–22 (2015)
38. McGeer, T.: Passive dynamic walking. Int. J. Robot. Res. **9**, 62–82 (1990)
39. McGhee, R.B.: Some finite state aspects of legged locomotion. Math. Biosci. **2**, 67–84 (1968)
40. Moldovan, F., Dolga, V., Ciontos, O., Pop, C.: Cad design and analytical model of a twelve bar walking mechanism. Sci. Bull. - "Politeh." Univ. Buchar., Ser. D Mech. Eng. **73**(2), 35–48 (2011)
41. Nicolaescu, L.I.: An Invitation to Morse Theory. Springer, Berlin (2011)
42. Nikravesh, P.E.: Computer-Aided Analysis of Mechanical Systems. Prentice Hall International, Englewood Cliffs (1988)
43. Nikravesh, P.E.: Planar Multibody Dynamics: Formulation, Programming and Applications. CRC Press, Florida (2007)
44. Obayashi, I., Aoi, S., Tsuchiya, K., Kokubu, H.: Common formation mechanism of basin of attraction for bipedal walking models by saddle hyperbolicity and hybrid dynamics. Jpn. J. Ind. Appl. Math. **32**, 315–332 (2015)
45. Perko, L.: Differential Equations and Dynamical Systems. Springer, Berlin (2001)
46. Plecnik, M.M., McCarthy, J.M.: Numerical synthesis of six-bar linkages for mechanical computation. J. Mech. Robot. **6**(3), 012 (2014)
47. Plecnik, M.M., McCarthy, J.M.: Kinematic synthesis of Stephenson III six-bar function generators. Mech. Mach. Theory **97**, 112–126 (2016)
48. Raibert, M.H., Brown, H.B. Jr, Chepponis, M., Koechling, J., Hodgins, J.K., Dustman, D., Borvansky, L.: Dynamically stable legged locomotion. Technical Report 1179, LL–6, MIT Artificial Intelligence Laboratory (1989)
49. Roy, S.S., Pratihar, D.K.: Study on energy consumption in turning motion of hexapod walking robots. In: Proceedings of the World Congress on Engineering, vol. I, pp. 1511–1516 (2011)
50. Roy, S., Pratihar, D.: Effects of turning gait parameters on energy consumption and stability of a six-legged walking robot. Robot. Auton. Syst. **60**(1), 72–82 (2012)
51. Roy, S.S., Pratihar, D.K.: Dynamic modeling, stability and energy consumption analysis of a realistic six-legged walking robot. Robot. Comput.-Integr. Manuf. **29**(2), 400–416 (2013)
52. Roy, S.S., Pratihar, D.K.: Kinematics, dynamics and power consumption analyses for turning motion of a six-legged robot. J. Intell. Robot. Syst. **74**(3), 663–688 (2014)
53. Schiehlen, W.: Multibody Systems Handbook. Springer, Berlin (1990)
54. Schiehlen, W.: Multibody system dynamics: roots and perspectives. Multibody Syst. Dyn. **1–2**, 149–188 (1997)
55. Schiehlen, W.: Energy-optimal design of walking machines. Multibody Syst. Dyn. **13**, 129–141 (2005)
56. Schiehlen, W.: Research trends in multibody system dynamics. Multibody Syst. Dyn. **18**(1), 3–13 (2007)

57. Seok, S.: Highly parallelized control programming methodologies using multicore CPU and FPGA for highly dynamic multi-dof mobile robots, applied to the MIT Cheetah. Ph.D. thesis, Massachusetts Institute of Technology, Department of Mechanical Engineering (2014)
58. Shabana, A.A.: Dynamics of Multibody Systems. Cambridge University Press, New York (1989)
59. Silva, M.P., Ambrósio, J.A.C.: Kinematic data consistency in the inverse dynamic analysis of biomechanical systems. Multibody Syst. Dyn. **8**(2), 219–239 (2002)
60. Sitti, M., Menciassi, A., Ijspeert, A.J., Low, K.H., Kim, S.: Survey and introduction to the focused section on bio-inspired mechatronics. IEEE/ASME Trans. Mechatron. **18**(2), 409–418 (2013)
61. Steindl, A., Troger, H.: Dimension reduction: a key concept in dynamics. In: The Sixth EUROMECH Nonlinear Dynamics Conference, ENOC, 2008 (2008)
62. Stejskal, V., Valášek, M.: Kinematics and Dynamics of Machinery. Dekker, New York (1996)
63. Talebi, S., Poulakakis, I., Papadopoulos, E., Buehler, M.: Quadruped robot running with a bounding gait. In: Experimental Robotics, vol. VII, pp. 281–289 (2001)
64. van der Schaftn, A., Schumacher, H.: An Introduction to Hybrid Dynamical Systems. Lecture Notes in Control and Information Sciences, vol. 251. Springer, Berlin (2000)
65. Weyand, P.G., Bundle, M.W., McGowan, C.P., Grabowski, A., Brown, M.B., Kram, R., Herr, H.: The fastest runner on artificial legs: different limbs, similar function? J. Appl. Physiol. **107**, 903–911 (2009)
66. Witten, E.: Supersymmetry and Morse theory. J. Differ. Geom. **17**, 661–692 (1982)